

# The Star Formation History and the Morphological Evolution of the Draco Dwarf Spheroidal Galaxy

Antonio Aparicio

Instituto de Astrofísica de Canarias, E38205-La Laguna, Tenerife, Canary Islands, Spain

Departamento de Astrofísica, Universidad de La Laguna, E38200 - La Laguna, Tenerife, Canary Islands, Spain

Ricardo Carrera

Instituto de Astrofísica de Canarias, E38205-La Laguna, Tenerife, Canary Islands, Spain

David Martínez-Delgado

Instituto de Astrofísica de Canarias, E38205-La Laguna, Tenerife, Canary Islands, Spain

## ABSTRACT

The photometric and morphological properties, as well as the star formation history, of the Draco dwarf spheroidal galaxy are analyzed on the basis of wide field, CCD photometry of the resolved stars covering about  $1^{\circ}2$ .

Draco is at a distance  $d = 80 \pm 7$  kpc and has a metallicity,  $[\text{Fe}/\text{H}]$ , of  $-1.8 \pm 0.2$ . No metallicity gradient is detected. The star surface density distribution can be fitted by a single exponential law of scale-length  $\alpha = 5'0 \pm 0'1$ . The central surface magnitude is  $\mu''_{V''} = 24.4 \pm 0.5$  and the core radius  $r_c = 7'5 \pm 0'3$  (equivalent to  $r_c = 175 \pm 7$  pc). Within errors, the same scale-lengths are found for the density profiles along the semi-major axis and the semi-minor axis (re-scaled to semi-major axis units, using the ellipticity of the galaxy) of Draco. There are hence no evidences of a tidal-tail associated to Draco. The tidal radius of the galaxy is found to be  $r_t \simeq 42'$  ( $\simeq 1$  kpc).

The possibility that the large mass-to-light relation in Draco could be accounted for by a convenient spatial orientation is tested. An upper limit to Draco's size along the line of sight is  $\sim 14$  kpc. This is too small to account for the velocity dispersion of Draco if it were due to projection effects only, and implies that other mechanisms (e.g., dark matter) are required.

The stellar population of Draco is mainly old. Although some intermediate-age population is present in Draco, most of the star formation (up to 90%) took place before  $\sim 10$  Gyr ago. No significant star formation activity is detected in the last  $\sim 2$  Gyr. Two methods (*partial model* and *subgiant*) have been used to investigate the star formation history of Draco, both producing results in good qualitative agreement.

No difference is found between the scale lengths of the distributions of old ( $\gtrsim 9$  Gyr) and young ( $\sim 2$ – $3$  Gyr) stars, indicating either that both populations were formed under the same kinematic conditions, or that any initial difference was afterwards erased.

*Subject headings:* galaxies: dwarf — galaxies: fundamental parameters — galaxies: individual (Draco) — galaxies: spheroidal — galaxies: stellar content — galaxies: structure

## 1. Introduction

In contrast with the early, simple idea that dwarf spheroidal (dSph) galaxies were systems essentially consisting of old, globular cluster-like, Population II stars (Baade 1963), they have been revealed as objects having undertaken complex star formation processes during their lives (Mighell & Rich 1996; Hurley-Keller, Mateo, & Nemec 1998; Stetson, Hesser, & Smecker-Hane 1998; Martínez-Delgado, Gallart, & Aparicio 1999; Gallart *et al.* 1999b). Indications that dSphs could contain some intermediate-age or young stars were early found by Baade & Swope (1961). Since then, other proofs have been accumulated, such as the presence of carbon stars (Aaronson & Mould 1980; Mould *et al.* 1982; Frogel *et al.* 1982; Azzopardi, Lequeux, & Westerlund 1986) and bright AGB stars (Elston & Silva 1992; Freedman 1992; Lee, Freedman, & Madore 1993; Davidge 1994; but see also Martínez-Delgado & Aparicio 1997). Stellar evolution theory became increasingly important in the interpretation of the color–magnitude diagrams (CMDs) when these reached the turn-offs of intermediate-age and old stars (see Mould & Aaronson 1983 and Mighell 1997 for the Carina dSph and Aparicio 1998 for a review). Comparison with theoretical isochrones allowed the determination of the range of ages present in the galaxies. DSph galaxies were studied with these techniques and the idea that all them, in one way or another, have a composite stellar population and that no two dSphs could be identified to have similar star formation histories (SFHs) became popular. In later years, the most powerful way to obtain the SFH, namely the analysis of the CMD with synthetic CMDs computed from a stellar evolution library (Aparicio 2001), has confirmed the wide variety of scenarios and has revealed complex, frequently bursting SFHs in dSphs (Hurley-Keller *et al.* 1998; Mighell 1997; Martínez-Delgado *et al.* 1999; Gallart *et al.* 1999b; Hernández, Gilmore, & Valls-Gabaud 2000; Aparicio 2001).

Structurally, dSphs are usually well fitted by King models, although exponential fittings are also adequate (Irwin & Hatzidimitriou 1995). They show relatively small scale lengths and have low central surface brightness (Gallagher & Wise 1994). They are the least-massive galaxies known, but still, their velocity dispersions imply mass-to-luminosity relations,  $\Upsilon$ , as large as  $100 \Upsilon_{\odot}$ . This is usually explained as dSphs containing large amounts of dark matter, but whether or not they are really bound systems (Gallagher & Wise 1994) and whether or not the large values of  $\Upsilon$  are due to peculiar orientation in space (Kroupa 1997; Klessen & Kroupa 1998) is still subject of discussion. What is clear is that at least some dSphs, such as Sagittarius (Mateo, Olszewski, & Morrison 1998; Martínez-Delgado *et al.* 2001a) or Ursa Minor (Martínez-Delgado *et al.* 2001b) show evidences of undergoing a process of tidal disruption by the Milky Way. This

would eventually be related to the galaxy formation predicted in cold dark matter scenarios, in which dwarf galaxies would be the first to form and would subsequently be merged into larger systems (White & Rees 1978).

Several efforts have been devoted to the study of Draco. It was discovered by Wilson (1955) and was the subject of a careful photographic analysis leading to its first CMD by Baade & Swope (1961). They found several RR Lyrae variables and noticed that the horizontal branch (HB) was predominantly populated in the red part but also had a blue component. They were also the first to find anomalous Cepheids, later identified in other dSph galaxies. Stetson (1979a) published new photographic photometry and estimated the distance modulus to be  $(m - M)_0 = 19.4$  from the magnitude of the HB. Deeper CMDs were obtained by Stetson, VandenBergh, & McClure (1985), who reached the turn-off of the dominant, old population about 3.5 mag below the HB. Carney & Seitzer (1986) found unambiguous evidence of a blue plume of stars above the main turn-off, as well as possible traces of an 8 Gyr-old stellar population. Recently, Grillmair *et al.* (1998) have presented WFPC2 *HST* photometry that allows the MS luminosity function down to 3 mag below the oldest turn-off to be determined.

The stellar density distribution of Draco was early studied by Hodge (1964) and, more recently, by Irwin & Hatzidimitriou (1995) who report a tidal radius of  $28'$  and by Lake (1990), Pryor & Kormendi (1990) and Piatek *et al.* (2001) who find evidences of a larger extension of the galaxy.

Draco's metallicity has been found to be very low. From the color of the RGB, Carney & Seitzer (1986) estimated it to be  $[\text{Fe}/\text{H}] \simeq -2$  with a dispersion of 0.8 dex. This is in good agreement with spectroscopic results for several giant stars, which lead to  $-3 < [\text{Fe}/\text{H}] < -1.5$  (Stetson 1984; Shetrone, Bolte, & Stetson 1998);  $[\text{Fe}/\text{H}] = -1.9 \pm 0.4$  (Lehnert *et al.* 1992) or  $[\text{Fe}/\text{H}] = -2.00 \pm 0.21$  (Shetrone, Côté, & Sargent 2001). This studies also clearly establish a high metallicity dispersion of the order of 1 dex.

Since the early work by Baade & Swope (1961), the SFH of Draco has been the subject of much discussion. The position and morphology of its RGB would indicate a very old age for the main population, similar to that of the globular clusters (Grillmair *et al.* 1998). But the predominantly red HB seems to be incompatible with this, at least if age is the second parameter (although recent results indicate that this assumption might be inadequate: Rosenberg *et al.* 1999; Behr *et al.* 2000). In such a case, Draco should be some 2 Gyr younger than both the globular clusters and the Ursa Minor dSph galaxy (Stetson *et al.* 1985; Carney & Seitzer 1986). On another hand, Carney & Seitzer (1986) found some evidence of a younger,  $\sim 8$  Gyr-old population and, if the blue plume is produced by younger MS stars rather than by blue stragglers, in favor of the hypothesis that the star formation in Draco should be extended up to a few Gyr ago, even if at a low rate (Carney & Seitzer 1986; Grillmair *et al.* 1998). This would also be compatible with the presence of the aforementioned anomalous Cepheids, which would belong to a few Gyr-old population (Norris & Zinn 1975; Demarque & Hirshfeld 1975; see also Gallart *et al.* 1999a and

references therein).

In this paper we present an analysis of the star formation history, metallicity, and morphological properties of Draco, based on wide-field, ground-based photometry. We confirm previous results favoring a predominantly old stellar population and show evidence of a relatively short star formation burst 2–3 Gyr ago. The paper is organized as follows. In §2, the observations and the data reduction are presented. In §3, the CMD of Draco is presented and the metallicity and distance obtained. In §4, the morphological properties of Draco are discussed, including its overall structure, surface luminosity distribution and three-dimensional orientation. In §5, the star formation history is computed using two different methods. Finally, the main results of the paper are summarized in §6.

## 2. Observations and data reduction

Images of Draco were obtained in  $B$  and  $R$  Johnson–Cousins filters during several observing runs with the INT (2.5 m) at Roque de los Muchachos Observatory on the island of La Palma (Canary Islands, Spain). Table 1 gives the journal of observations. The WFC was used with four  $2048 \times 4096$  EEV chips. The scale is  $0.33''/\text{pix}$  which provides a total field of about  $35 \times 35$  arcmin $^2$ . Several fields were sampled, as shown in Fig. 1. Figure 2 displays an isopleth map of Draco, by Irwin & Hatzidimitriou (1995), showing also the area covered by our observations. Total integration times were 1920 s in  $B$  and 1600 s in  $R$  for field A (the central field); 3600 s in  $B$  and 4200 s in  $R$  for field B, and 2820 s both in  $B$  and  $R$  for field C.

Bias and flat-field corrections were made with IRAF. Then, DAOPHOT and ALLFRAME (Stetson 1994) were used to obtain the instrumental photometry of the resolved stars. Transformation into the standard photometric system requires several observations of standard star fields in such a way that standards are measured in all four chips. In practice, we observed three fields in the four chips and used them to calculate relative photometric transformations from each chip to the central one (chip 4). Then, a larger number of standard star fields were measured in chip 4 during the observing run to calculate both nightly atmospheric extinctions and the general transformation into the standard Johnson–Cousins system. In total, 280 measurements of 30 standards were made during the observing run of June 1999. Summarizing, the transformations from each chip to chip 4 are:

$$(b_4 - b_1) = 0.36 - 0.01(B - R); \quad \sigma = 0.01, \quad (1)$$

$$(r_4 - r_1) = 0.45 + 0.04(B - R); \quad \sigma = 0.02, \quad (2)$$

$$(b_4 - b_2) = 0.409 - 0.003(B - R); \quad \sigma = 0.007, \quad (3)$$

$$(r_4 - r_2) = 0.462 + 0.102(B - R); \quad \sigma = 0.003, \quad (4)$$

$$(b_4 - b_3) = 0.438 - 0.024(B - R); \quad \sigma = 0.008, \quad (5)$$

and

$$(r_4 - r_3) = 0.48 + 0.06(B - R); \quad \sigma = 0.03, \quad (6)$$

where subindices refer to chips, lower-case letters stand for instrumental magnitudes, and capital letters for Johnson–Cousins magnitudes. The  $\sigma$  values are the dispersions of the fits at the centers of mass of the point distributions; hence they are the minimum internal zero-point errors. There is a large zero point (bigger than 0.4 mag in most cases) displacement between chip 4 and the other chips, which implies the lower sensitivity of the former.

Transformations from chip 4 instrumental magnitudes measured at the top of the atmosphere into Johnson–Cousins magnitudes are given by:

$$(B - b_4) = 24.603 + 0.036(B - R); \quad \sigma = 0.006 \quad (7)$$

and

$$(R - r_4) = 24.504 + 0.040(B - R); \quad \sigma = 0.010, \quad (8)$$

where, as before, lower-case letters refer to instrumental magnitudes and capital letters to Johnson–Cousins magnitudes. Finally, dispersions of the extinctions for each night are about  $\sigma = 0.01$  for both filters.

This provides the photometric transformation for the 1999 observing run. For the remaining runs, transformations were done using as secondary standards the stars of the Draco fields overlapping with those of the 1999 run. In this way, the consistency of the photometric scales of the different fields is secured.

Aperture corrections are necessary to transform the ALLFRAME magnitudes into large-radius aperture magnitudes. The latter is the system in which the magnitudes of standard stars have been measured. The transformation has been performed through aperture photometry on a set of  $\sim 200$  isolated bright stars of field A after subtracting the remaining stars from the frames. The difference between these and the ALLFRAME magnitudes for the same stars provides the aperture correction for the corresponding frame. Dispersions in the aperture corrections are of the order of 0.01. Putting all the errors together, the total zero-point error of our photometry can be estimated to be about  $\sigma = 0.02 - 0.03$  for both bands, although it is up to  $\sigma = 0.04$  for chip 3 in filter  $R$ .

For each star, ALLFRAME provides with the dispersion in the PSF fitting. In general, these dispersions do not reproduce the external errors of the photometry, which stem mainly from stellar crowding and blending (see Aparicio, & Gallart 1995 and Gallart, Aparicio, & Vilchez 1996), but they provide an indication of the internal accuracy of the photometry. In this sense, our average ALLSTAR errors are 0.02, 0.06, and 0.15 for  $R = 21.1$ , 22.8, and 23.9, respectively, and for  $B = 22.5$ , 23.9, and 25.0, respectively.

Artificial-star tests were performed on field A in the usual way (Stetson & Harris 1988; see also Aparicio & Gallart 1995) to check the observational effects and estimate completeness factors as a function of magnitude. In practice, 20 000 artificial stars were added to the  $B$  and  $R$  images of Draco. Coordinates of these stars were distributed in a grid covering the whole image. The step used to build this net was  $7''$  both in  $x$  and  $y$ , avoiding overcrowding effects. Colors and magnitudes of artificial stars were obtained from the synthetic CMD (computed as described in Aparicio & Gallart 1995) of an old stellar population. In this way, they approximately mimic the real CMD of Draco, which is important for a realistic observational effect test. The resulting completeness factors are shown in Figure 3. They start to drop at " $V$ "  $\simeq 23.0$  (with " $V$ " =  $(B + R)/2$ ; see §3.1). But about 5% of the stars are lost at any magnitude brighter than " $V$ "  $\simeq 23.0$ . These are mostly stars lying in the regions around very bright, saturated, field stars.

### 3. The stellar content, metallicity and distance of Draco

#### 3.1. The color-magnitude diagram

Figure 4 shows the CMD of Draco. Stars within the inner  $30'$  (the semi-major axis) have been plotted (see below). A pseudo- $V$  magnitude, obtained as " $V$ " =  $(B + R)/2$ , is used in the vertical axis. This has the advantage of producing an almost horizontal HB. It shows a well populated, narrow red giant branch (RGB) with a relatively small slope as well as a blueward extended HB. These features are the trace of an old, low-metallicity stellar population with a small metallicity dispersion. The main sequence (MS) is visible at " $V$ "  $> 23$  and, very interestingly, an extended sequence of blue stars with " $V$ "  $< 23$ ,  $(B - R) < 0.6$  is also present. This could be a blue-straggler (BS) sequence or the signature of a younger stellar population.

Figure 5 shows CMDs for elliptical annuli of increasing semi-major axis. Note firstly that traces of Draco RGB and MS are still evident at  $20' < a < 42'$ . Also noticeable is the small group of stars above the red part of the horizontal branch, visible in the CMD for  $a < 7/farcm5$  at " $V$ "  $\simeq 19.7$ ,  $(B - R) = 1.0$ . This can be a red clump formed by stars burning He in their nuclei and would be the signature of a young-to-intermediate population. In fact, Baade & Swope (1961) and Zinn & Searle (1976) found anomalous Cepheids in this region. An explanation for the origin of these variables is indeed that they are young-to-intermediate age stars. If so, they should have an MS counterpart, perhaps like the blue extension discussed above. We will come again to this point in Section 4.

These CMDs will be used later on as a reference for discussion of galactocentric gradients of stellar populations and metallicity.

### 3.2. The metallicity

The metallicity of Draco has been investigated by Carney & Seitzer (1986), who obtained  $[\text{Fe}/\text{H}] = -2$  from the color of the RGB. From the spectroscopy of three giant stars, Shetrone *et al.* (1998) found that the metallicity should be in the range  $-3.0 < [\text{Fe}/\text{H}] < -1.5$ .

The color of the RGB is frequently used to obtain an alternative estimate of the metallicity. Recently, Gallart *et al.* (2001) have shown that these values can be wrong. However we have applied the method to our data and derived an estimate of the metallicity in the understanding that it will be useful for comparison with results for other galaxies existing in the literature.

To do so, we have used the relations provided by Saviane *et al.* (2000), based on the position of the RGB of several globular clusters. However, these relations are calculated in the  $[\text{M}_V, (\text{V} - \text{I})]$  plane while our photometry is  $\text{BR}$ . Hence the Saviane *et al.*'s relations must be transformed into the  $[\text{M}_R, (\text{B} - \text{R})]$  plane to be used with our data.

For this we have used the Padua (Bertelli *et al.* 1994) and Yale (Yi, Demarque, & Oemler 1997) isochrones to obtain, for a set of metallicities, the values of the absolute  $\text{M}_R$  magnitude and the color indices corresponding to the RGB at  $\text{M}_I = -3$ . We denote these values by  $\text{M}_{R_{I=-3}}$ ,  $(\text{V} - \text{I})_{I=-3}$  and  $(\text{B} - \text{R})_{I=-3}$ , respectively. In this way, we obtain the curve in the  $[\text{M}_R, (\text{B} - \text{R})]$  plane shown by a thick line in Figure 6. Besides  $\text{M}_{R_{I=-3}}$  and  $(\text{B} - \text{R})_{I=-3}$ , the parameter changing along this curve is  $(\text{V} - \text{I})_{I=-3}$ . The intersection of the RGB fiducial line of Draco with the curve gives its  $(\text{V} - \text{I})_{I=-3}$ , whose value is 1.18. When this is introduced into the Saviane *et al.* (2000) relations, the metallicity is obtained to be  $[\text{Fe}/\text{H}] = -2.0 \pm 0.1$  if the Zinn & West (1984; ZW from here on) metallicity scale is used, or  $[\text{Fe}/\text{H}] = -1.6 \pm 0.1$  if the Carretta & Gratton (1997; CG from here on) metallicity scale is used.

Besides this, we have directly obtained an alternative calibration for the metallicity in the  $[\text{M}_R, (\text{B} - \text{R})]$  plane. For this purpose, we have used the RGBs of three globular clusters: NGC 1904 (Alcaino *et al.* 1994), NGC 4590 (Alcaino *et al.* 1990), and NGC 6723 (Alcaino *et al.* 1999). A summary of the metallicity (according to scales for the globular cluster metallicities by ZW and CG), the distance and the reddening of these clusters is given in Table 2. In accordance with Saviane *et al.* (2000), the cluster RGBs have been fitted by a hyperbolic equation of the form  $y = a + bx + c/(x - d)$ . This fit has then been used to calculate the color index  $(\text{B} - \text{R})$  for  $\text{M}_{R=-2.5}$ , which we will denote  $(\text{B} - \text{R})_{R=-2.5}$ . Finally, the relation between the metallicity and  $(\text{B} - \text{R})_{R=-2.5}$  has been determined for both the ZW and CG scales. For the second case, a linear fit of the form  $[\text{Fe}/\text{H}] = a(\text{B} - \text{R})_{R=-2.5} + b$  is enough, but for the ZW scale, a quadratic fit of the form  $[\text{Fe}/\text{H}] = a(\text{B} - \text{R})_{R=-2.5}^2 + b(\text{B} - \text{R})_{R=-2.5} + c$  is preferable. The coefficients of the fits are given in Table 3.

The metallicities obtained are  $[\text{Fe}/\text{H}] = -1.9 \pm 0.1$  if the ZW metallicity scale is used or  $[\text{Fe}/\text{H}] = -1.6 \pm 0.1$  if the CG scale is used.

Considering all the values obtained here, we adopt  $[\text{Fe}/\text{H}] = -1.8 \pm 0.2$  for the metallicity of

Draco. Figure 7 shows the RGBs of the three clusters used to calculate the  $[\text{Fe}/\text{H}] - (B - R)_{R=-2.5}$  relation superimposed on the CMD of Draco, and demonstrates that, in fact, the metallicity of the galaxy should be between the NGC 4590 and NGC 1904 values.

$(B - R)_{R=-2.5}$  and the metallicity obtained therefrom can be used to test whether galactocentric metallicity gradients exist in Draco. CMDs for elliptical annuli of increasing semi-major axis, similar to those shown in Fig. 5, have been used to this purpose. Third-degree polynomial fits to points in the interval  $-1.5 \leq R \leq -3.2$  were used to obtain a fiducial RGB for each CMD. The  $(B - R)_{R=-2.5}$  values for each one are represented in Figure 8. The error bars show the internal dispersions of points about the polynomial fits. Inspection of this figure reveals that no metallicity gradient can be deduced to exist in Draco.

A metallicity dispersion of about 1 dex in  $[\text{Fe}/\text{H}]$  has been clearly established in studies referred to the inner  $\sim 5'$  of Draco (Stetson 1984; Shetrone, Bolte, & Stetson 1998; Lehnert *et al.* 1992; Shetrone, Côté, & Sargent 2001). Note that this is not in contradiction with the absence of an overall, large-scale metallicity gradient found here.

### 3.3. The distance

Previous estimates of Draco's distance have been made by Stetson (1979a), who obtained  $d = 72 \pm 3$  kpc using the position of the red HB, and by Nemec (1984), who obtained  $d = 84 \pm 12$  kpc using RR Lyr variability periods. Using our data, the distance to Draco can be estimated through the magnitude of the HB at the RR Lyrae instability strip. From an analytical fit to the blue part of the HB we have estimated that magnitude to be  $"V" = 20.2 \pm 0.1$ . A shift has to be applied to this value to obtain the actual  $V$  magnitude. Considering the  $BVR$  magnitudes in the RR Lyrae instability strip given by the Padua stellar evolution library, that shift is  $"V" - V = 0.06$ , hence  $V = 20.14$ . Finally, using the relation by Lee *et al.* (1999) for the luminosity-metallicity of the HB,  $M_V = 0.17[\text{Fe}/\text{H}] + 0.82$ , the distance becomes  $(m - M)_V = 19.6 \pm 0.2$ , where the quoted error includes uncertainties in the  $"V" - V$  transformation, as well as the metallicity error. Reddening for Draco was investigated by Stetson (1979b), who found  $E(B - V) = 0.03 \pm 0.01$ . It can also be calculated from the IR maps of dust by Schlegel, Finkbeiner, & Davis (1998), which give  $E(B - V) = 0.028$ , corresponding to an extinction of  $A_V = 0.09$ . Applying this correction to the distance modulus gives  $(m - M)_0 = 19.5 \pm 0.2$ , or  $d = 80 \pm 7$  kpc. We will adopt this value.

## 4. The morphological properties of Draco

### 4.1. Density profile

The radial stellar density distribution of Draco was first obtained from wide-field photographic photometry by Hodge (1964), who reported a tidal radius  $r_t = 26'$ , and more recently by Irwin &

Hatzidimitriou (1995), who derived  $r_t = 28'$ . Lake (1990) and Pryor & Kormendi (1990) modeled the galaxy using Hodge's data and found  $r_t = 55'$  and  $r_t = 36'$ , respectively. Very recently, Piatek *et al.* (2001) have carried out an extensive search of Draco stars beyond the Irwin & Hatzidimitriou (1995) tidal radius, finding evidence of the existence of such stars.

Here we provide a new profile, now based on CCD photometry. Three stellar distributions have been obtained from star counts in elliptical annuli of increasing semi-major axis. The eccentricity of the elliptical annuli has been assumed to be  $\epsilon = 1 - b/a = 0.29$  and the position angle  $82^\circ$ , after Irwin & Hatzidimitriou (1995). The center of the galaxy given by these authors has also been adopted. The three density profiles have been computed as follows. For the first one, all the resolved stars have been used. For the other two, only stars in two regions of the CMD where the ratio of Draco to foreground stars is largest, have been considered: the MS and the RGB. To sample the MS, stars within the box defined by  $0.6 < (B - R) < 1.0$ ;  $24.25 <'' V'' < 22.75$  have been used. For the RGB, box 14, as defined in Figure 13, has been used.

The final star density distributions are shown in Figure 9. The corresponding " $V$ " surface magnitude is given in the right-hand vertical scale, according to the magnitude scale obtained below. In all the cases, open circles show the raw distributions. The sky contamination by foreground and background objects must be subtracted from this to obtain the distribution of Draco stars. Background, extended objects are automatically removed by DAOPHOT, while background, stellar-shaped objects are indistinguishable from foreground stars. For this reason, from here on, we will refer to foreground contamination only, understanding that it include also the background stellar-shaped objects not rejected by DAOPHOT.

The raw radial surface density distributions (Fig. 9, open circles) change slope at  $a \simeq 20' - 25'$ , but continue decreasing until at least  $a \simeq 42'$ . Let assume that the sky star density has been reached at this distance. If the average densities for  $a > 42'$  are subtracted from the raw radial distributions, the profiles shown by full dots in Figure 9 are obtained. A single law can account for the density profile for  $a > 5'$  in all the cases. On the one hand, the absence of a plateau for large galactocentric distances indicates that a tidal tail is not present in Draco. On the other hand, this indicates that the tidal radius (semi-major axis) of Draco is about  $r_t = 42'$ .

A way to further explore the presence of extra-tidal stars or of a tidal tail structure is to compare the density profiles in the direction of the major and minor axes. We have done so for the MS and the RGB stars, for which the Draco-to-foreground star ratio is greater. The results are shown in Figure 10. The distributions obtained from star counting in full ellipses (the same shown in Fig. 9, full dots) are compared with those for stars within two strips along the western semi-major axis and the southern semi-minor axis. Table 4 lists the scale-lengths in each case (column 2). For the semi-minor axis, these quantities have been scaled into units along the semi-major axis; i.e., they have been divided by  $b/a$ , so that they are directly comparable with the scale-lengths corresponding to the semi-major axis and full ellipses. No significant differences are found in either case, which leads to the conclusion that Draco is a very extended, low density

galaxy, but that no evidence of a tidal tail populated by stars stripped away from the galaxy are found. In any case, more data about the stellar population in fields around Draco’s main body are required to better understand the galaxy’s structural properties.

Finally, the core radius (semi-major axis) is  $r_c = 7'5 \pm 0'3$ . At the distance adopted for Draco, this corresponds to  $r_c = 175 \pm 7$  pc.

## 4.2. Surface photometry

It is difficult to obtain the surface brightness distribution of galaxies which, like Draco, have a very low stellar density and which are resolved down to stars of quite faint intrinsic luminosity. An indirect technique is to obtain the surface density distribution of resolved stars, which is afterwards transformed into a surface-brightness scale. In our case, this transformation has been done as follows. Firstly, a synthetic model for a stellar population as found for Draco in §5 has been computed. Secondly, the number of RGB stars has been counted in this model. To do this, stars in box 14 (see Figure 13) have been considered. Finally, comparison of this number with the total luminosity in  $B$  and  $R$  for the synthetic model provides a scale transformation from RGB star counts to magnitudes. The accuracy of the final scale of magnitudes cannot be expected to be high. In particular, it depends on the assumed IMF. But it is probably better than that obtained through direct measurement of brightness on a big field dominated by background noise and contamination by bright foreground stars.

Applying this method, we estimate the central surface brightness in  $B$ ,  $R$ , and “ $V$ ” to be  $\mu_{B,0} = 25.0 \pm 0.5$ ,  $\mu_{R,0} = 23.9 \pm 0.5$  and  $\mu_{“V”,0} = 24.4 \pm 0.5$ , where the quoted errors should account for the high degree of uncertainty. Irwin & Hatzidimitriou (1995) obtained  $\mu_{V,0} = 25.5 \pm 0.5$ , which is one magnitude fainter than ours. It is difficult to say which value is preferable. Irwin & Hatzidimitriou have obtained theirs from a King model fit to photographic data. Our CCD photometry is deeper and is expected to be more accurate, but, as previously quoted, our estimate could be affected by a wrong choice of the IMF and, in general, by the fact that we are using a stellar population model. In our opinion, the relatively large disagreement between both values reveals nothing but the difficulty of obtaining accurate surface photometry of this kind of systems.

The integrated magnitudes of Draco can be obtained by integration of the density profile and the central surface brightness abovey obtained. The results, together with all the morphological parameters obtained here and several other integrated quantities are summarized in Table 5. In Table 6, morphological parameters are compared with other authors’ results.

### 4.3. Spatial distribution of stellar populations

The spatial distribution of stellar populations of different ages gives information on the time-scale in which stars mix out in the galaxy and on kinematic and/or morphological evolution. Computing the detailed models required to perform an accurate analysis is beyond the scope of this paper. But valuable information can be obtained from the comparison of the radial distribution scale lengths of populations of different ages. The latter can be selected from the boxes defined in Fig. 13, since different boxes sample different ages (see details in §5).

From synthetic models computed for the SFH study (see below, §5) it can be seen that boxes 12 and 14 (Fig. 13) contain stars with ages in the interval 9–15 Gyr, while boxes 2 to 6, 10 and 13 contain younger stars and preferably, stars in the interval 2–3 Gyr (they sample the small recent starburst; see §5). We have calculated the radial distribution scale length for both groups of stars in the region  $5' \leq a \leq 20'$ . We have obtained  $\alpha = 5'8 \pm 0'2$  for the older population and  $\alpha = 6' \pm 1'$  for the younger; *i.e.*, there is no significant difference either between both or with respect to the whole resolved stellar population. Within the errors, this indicates that stars of different ages where formed with similar spatial distribution or that their movement in the galaxy has completely mixed them.

### 4.4. On the three-dimensional orientation of Draco

Dwarf spheroidal galaxies usually present high mass-to-luminosity ratios ( $\Upsilon$ ). Draco, in particular, has  $\Upsilon = 84 \Upsilon_{\odot}$  (Mateo 1998). Dark matter is usually invoked as an explanation for these large values in a virialized scenario. An alternative explanation has been proposed by Kroupa (1997) and Klessen & Kroupa (1998), who suggest that tidal disruption of these galaxies by the Milky Way potential would well produce very elongated systems whose main axis, together with the main axis of the velocity ellipsoid, could eventually be oriented close to the line of sight. In such a case, the high observed velocity dispersion would not need of large quantities of dark matter to be accounted for.

To check this possibility we have adopted the hypothesis that Draco is configured according to model RS1-4 of Kroupa (1997), which is the one that most closely reproduces the  $\Upsilon$  of Draco. The spatial distribution of stars in this model is shown in Figure 11. We have then simulated the predicted distance dispersion of Draco stars to us in a synthetic CMD of a stellar population similar to that found for Draco (see §4). The CMDs before and after simulating the distance dispersion are shown in Figure 12. Comparison of the right-hand CMD with the Draco CMD (Fig. 4) clearly indicates the incompatibility of the RS1-4 model with the observations.

On another hand, the extension of Draco along the line of sight can be estimated from the width of the HB. This width is potentially affected by several factors, such as observational effects, stellar evolution or binarity of composite stellar populations. From our artificial-star test (§2) we

have checked that widening of the HB by observational effects can be neglected, but considering every other possible effect in detail is complicated. However, an upper limit estimate can still be set by neglecting all the effects and assuming that the entire width observed in the red HB (Fig. 4) is produced by distance dispersion. In such a case, the size of Draco along the line of sight would be  $\sim 14$  kpc. This is quite a large value compared with Draco's size in the plane of sky but it should be stressed that it is an upper limit, and that it is still less than 1/3 the size given by the RS1-4 model.

## 5. The Star Formation History

The SFH of a galaxy can be derived in detail from a deep CMD through comparison with synthetic CMDs (Aparicio 2001). Details on the computation of synthetic CMDs and on the method used here to derive the SFH can be found in Gallart *et al.* (1999b), Aparicio & Gallart (1995), and references therein. The accuracy and temporal resolution of the SFH depend on the quality and depth of the observed CMD and on the uncertainties in the stellar evolutionary library upon which the synthetic CMDs are computed. To obtain a reasonable resolution for old ages the CMD must sample stellar evolutionary phases sensitive to these ages, such as the HB or the lower MS. Moreover, the RC, the RGB, and the HB itself provide information on the chemical enrichment law (CEL).

The CEL and the initial mass function (IMF), together with the star formation rate (SFR), are the functions contained in the more general SFH. A function containing information on the fraction and mass distribution of binary stars would also be relevant. For simplicity, we have neglected here the influence of binary stars and have assumed a fixed IMF: that given by Kroupa, Tout, & Gilmore (1993). The CEL can be constrained by the morphology and color of the RGB. As discussed above (see §3.2) Draco presents a low average metallicity and a low metallicity dispersion,  $[Fe/H] = -1.8 \pm 0.2$ . This corresponds to  $0.0002 \leq Z \leq 0.0003$ . However, the Padua stellar evolutionary models produce a best fit to Draco RGB for  $Z \simeq 0.0005$ . This difference is due to the internal tuning of the stellar evolution models and is not important for the analysis of the metallicity. However, it is preferable using it to compute the synthetic CMDs necessary for the SFH study. In practice, we have assumed a CEL independent of time producing metallicity values for the stars randomly distributed in the interval  $0.0004 \leq Z \leq 0.0006$  for all ages. Provided that the stellar population does not have a large amount of young stars (younger than some 1 Gyr), as can be deduced from the extension of the MS of Draco, this CEL produces synthetic CMDs with an RGB always compatible with that of Draco.

The only remaining function to complete the SFH of Draco is the SFR. Two different methods have been used to obtain it. The first method is that of the IAC-Padua group (see Aparicio 1998 for a description and Gallart *et al.* 1999b for one of the latest applications), which we will refer to as the *partial diagram* or *partial model* method. The second method is that presented by Mighell (1997), which we will refer to as the *subgiant* method. We will discuss in turn the results obtained

with each of these.

### 5.1. The partial diagram method

This method was introduced by Aparicio, Gallart, & Bertelli (1997). To apply it, a few synthetic CMDs (partial models) are computed, each for a stellar population with ages in a narrow interval (typically, a few partial models are used each embracing an age interval ranging from several  $10^8$  yr to a few Gyr to cover the full  $\sim 15$  Gyr of galaxy ages). The Padua stellar evolution library (Bertelli *et al.* 1994) is used for this purpose. The basic idea is that any SFR can be simulated as a linear combination of partial models.

The practical way to derive the SFR is as follows. A number of boxes are defined in the CMDs (observed and partial models) and the number of stars are counted inside them. The boxes are defined in such a way they sample stellar evolutionary phases providing information about different ages. Let us call  $N_j^o$  the number of stars in box  $j$  in the observed CMD and  $N_{ji}^m$  the number of stars in box  $j$  of partial model  $i$  (the partial model covering the  $i$ th age interval). Using this, the distribution of stars in boxes of an arbitrary SFR can be obtained from a linear combination of the  $N_{ji}^m$ , by

$$N_j^m = k \sum_i \alpha_i N_{ji}^m. \quad (9)$$

The corresponding SFR can be written as

$$\psi(t) = k \sum_i \alpha_i \psi_p \Delta_i(t), \quad (10)$$

where  $\alpha_i$  are the linear combination coefficients,  $k$  is a scaling constant, and  $\Delta_i(t) = 1$  if  $t$  is inside the interval corresponding to partial model  $i$ , and  $\Delta_i(t) = 0$  otherwise. Finally, the  $\psi(t)$  having the best compatibility with the data can be obtained by a least-squares fitting of  $N_j^m$  to  $N_j^o$ , the  $\alpha_i$  coefficients being the free parameters.

The finite time interval of partial models introduces a limitation on the time resolution of the SFH. But it must be noted that the final limitation is indeed imposed by the accuracy of observations and the precision of stellar evolutionary models and also that increasing the time resolution of the computed solution is only a matter of computer time.

Ten partial models have been considered for the analysis of Draco SFH, covering the age interval from 15 to 2 Gyr. The latter has been assumed the youngest age present in the CMD because it is the age of the isochrone having the turn-off point at " $V$ "  $\sim 1.5$ , corresponding to the upper point of the Draco blue plume. On the other hand, 16 boxes have been defined in the CMD, as shown in Fig. 13, to characterize the distribution of stars. Boxes 1 to 6 sample the younger population, living in the upper MS. The consequences of this assumption are discussed below. In this analysis we will assume that all these stars are MS stars and not BS. Boxes 7 to 10 sample the subgiant (SG) region. The information provided by these stars is complementary to

the former one. Fainter stars are not considered because they are affected by bigger observational effects. In fact, this will limit the time resolution for the oldest stellar ages. Boxes 11 and 12 sample the HB. These boxes sample the old stellar population. In particular, if age is the second parameter, box 11 would contain the oldest pure population. Here, we will assume that this is the case, but it must be kept in mind that the nature of the second parameter is not fully confirmed and that the blueward extension of the HB depends on stellar evolution parameters that are not well controlled. The color uncertainty produced by this is the reason why we define boxes 11 and 12 to be quite extended in color.

Box 13 samples intermediate-age to young stars in the core He-burning phase. They should have a counterpart in the blue plume and the upper SG region. Region 14 samples the RGB, populated by old and intermediate-age stars born in fact in the full, 2–15 Gyr interval considered here, as well as some AGBs in the same age interval. Although it provides nothing in terms of age resolution when compared with the information contained in other boxes, the number of stars in box 14 is a strong tool to normalize the full SFR: independently of the age distribution, the integrated SFR for the old and intermediate-age stars must be compatible with the number of stars populating box 14. Box 15 samples intermediate-age AGBs. It should have a counterpart in the blue plume and the SG region. Finally, box 16 sample young AGBs. The fact that it contain no stars indicates that the SFR in the last several million years has been zero or negligible. Linear combinations of partial models predicting stars in this region will be automatically rejected.

We have so far commented qualitatively on the different age intervals sampled by each box defined in the CMD. However, the solution for the SFR is found in a global way, considering the number of stars in all the boxes. In practice, it is not reasonable to look for the best solution (the linear coefficients best reproducing the distribution of stars in the boxes of the observational CMD), but to search all the solutions providing a stellar distribution compatible with the observed one within some interval. Here, we have adopted as good solutions all those producing a number of stars in each box within  $2\sigma$  from the observed value,  $\sigma$  for each box being the maximum between  $(N_j^o)^{(1/2)}$  and 1. The reason for adopting a minimum value of 1 for  $\sigma$  is to dump small-number effects on the solution.

The resulting SFR is shown in Figure 14. Error bars represent the sigma value of all the linear combinations producing good solutions for each age interval. The most relevant fact of the solution is that the dominant population is old (older than 10 Gyr). It is also remarkable that the SFR extends down to a few Gyr-old stars, including a jump between 2 and 3 Gyr. The later depends on the assumption we have made that the blue plume is made up of normal MS stars. If this is wrong, the SFR of intermediate-age to young stars would be lower than the values obtained. However, the intermediate-age star formation activity is also supported by the presence of subgiants and core He-burning stars in the CMD.

This solution cannot be however considered as completely deterministic. In fact, error bars are in general comparable to the values of  $\psi(t)$  for ages between 3 and 10 Gyr. This, however,

does not mean that we know very little about the solution, but that we cannot determine with a high degree of confidence whether the most conspicuous population is 12–13.5 or 13.5–15 Gyr old, for example, or whether the jump at 2–3 Gyr is as strong as it appears in Fig. 14 or is more (or less) diluted in time.

Summarizing, the fact that the dominant population in Draco is old may be considered as a well established result of the present analysis. Also, under the assumption that the stars populating boxes 1 to 6 (Fig. 13) are MS stars rather than blue stragglers, a low rate, intermediate-age stellar population exist. The jump at 2–3 Gyr is compatible with an overpopulation of stars in box 4 but mainly comes from the stars populating box 13. These stars can well be  $\sim 1.2\text{--}1.5 M_{\odot}$  in the phase of core He burning.

The SFR obtained here has been used to calculate the total mass in stars and stellar remnants ( $M_{\star}$ ) for the inner 7.5 and 30' (semi-major axis). For this, it has been assumed that a fraction 0.8 of the integral of the SFR remains locked into stars or stellar remnants. The value obtained for 30' can be considered as a good estimate of the total real value, since the fraction of stars at distances larger than 30' is negligible (see Fig. 9). Both values are quoted in Table 5 and the second is used to calculate the dark matter fraction,  $\kappa$ .

## 5.2. The subgiant method

The turn-off is the most sensitive indicator of stellar age for single stellar populations. However, in systems such as galaxies, where the stellar population is composite, the turn-offs of successive stellar generations mix with each other and with the main sequence of younger stars. In such cases, the subgiant (SG) region is preferable for measuring stellar ages. It also has the advantage of being, for a given age and metallicity, above the corresponding turn-off point, thereby allowing a better signal to noise in the magnitudes.

Mighell (1997) introduced a simple method based on star counts in the SG region to determine the SFR. For this purpose, the SG region is divided with isochrones of a given metallicity and increasing ages. Then the number of stars are counted between each two isochrones, which provides a present-day age distribution. Normalized by the stellar lifetime in the SG region as a function of age, this distribution results in the SFR. In the present case, we perform this normalization dividing the observed, present-day age distribution by the distribution corresponding to a synthetic CMD computed for a constant SFR and the metallicity adopted for Draco.

Resolution is worse for older ages, due both to the increasing photometry errors and to the decreasing width of the magnitude interval between isochrones. The method provides a good time resolution up to  $\sim 8$  Gyr.

A severe limitation of the method, as it is presently applied, is that it allows only a constant metallicity for the stellar population. This, however, is not very important for very low metallicity

galaxies such as Draco. Also, as a matter of fact, this method uses only a part of the information that is used by the partial model method, for which the solution should be considered less accurate and conclusive. However, in the present case, in which metallicity evolution is not tested, the subgiant method provides an alternative approach in which the solution rest only on the SG stars.

In the present analysis, and for the same reasons as given in §4.1, the adopted metallicity was  $Z = 0.0005$ , with an He abundance of  $Y = 0.25$ . With this input and the Kroupa *et al.* (1993) IMF, a synthetic CMD has been computed for constant SFR in the age interval 1–15 Gyr. Observational effects have been simulated as explained in Aparicio & Gallart (1995). This is important because errors and completeness significantly change along the SG region. The simulation has been done six times with different random number seeds. This allows calculating a dispersion for the synthetic star counts in each age interval.

The SG region of Draco’s CMD is shown in Figure 15. Isochrones interpolated from the Padua library (Bertelli *et al.* 1994) are shown. The resulting SFR is presented in Fig. 16, which, together with a dominant old population, shows an intermediate-age population as far as 2 Gyr ago. To estimate the errors two components have been considered. The first is just the square root of the star counts for each age interval. It would account for the fact that we work with a limited number of stars. The second is the dispersion found for the synthetic star counts and would account for the random fluctuations in the observational effect simulation.

The most interesting thing is that both the partial model and the subgiant methods produce qualitatively similar results, including the young bump which, although less clear, is also visible in Fig. 16, slightly shifted to older ages. This stress the stability of the solution and reinforces the capability of both methods to obtain the SFH of nearby galaxies. The main difference is that the SFR derived by the subgiant method is more softly decreasing and it maintains a higher value at intermediate ages. This could be due to observational effects that would spread the stars in the subgiant region, the overall result being that fainter stars are moved upwards. In any case, the fact that the partial model method uses more information from the CMD eventually makes preferable the result obtained with it.

## 6. Conclusions

We have presented a photometric and morphological analysis of the Draco dwarf spheroidal galaxy, as well as a study of its stellar content and star formation history based on wide field photometry covering about  $1^\circ \times 1^\circ$ .

Two methods (*partial model* and *subgiant*) have been used to investigate the SFH of Draco. The most important result is that the stellar population is fundamentally old (older than  $\sim 10$  Gyr). Some 90% or 75% (depending on the method) of the star formation in Draco took place before  $\sim 10$  Gyr ago. After that, the star formation continued at a low rate and, apparently, a small burst was produced some 2–3 Gyr ago. No star formation activity is detected in the analysis

of the CMD for more recent epochs.

Several morphological and global parameters have been calculated for Draco. Its distance is  $d = 80 \pm 7$  kpc and its metallicity,  $[\text{Fe}/\text{H}] = -1.8 \pm 0.2$ . No metallicity gradient is detected along the galaxy.

The star surface density distribution of Draco can be fitted by a single exponential law of scale-length  $\alpha = 5'0 \pm 0'1$ , for galacto-centric distances larger than  $5'$ . Within errors, the same scale is found for the old (older than  $\sim 9$  Gyr) and the young ( $\sim 2\text{--}3$  Gyr) stars, indicating either that both populations were formed under the same kinematic conditions or that any initial difference was afterwards erased.

Evidences have been found of the galaxy extending as far as  $42'$  (1 kpc) from its center. This is in good agreement with the discovery by Piatek *et al.* (2001) of stars belonging to Draco beyond the previous tidal radius estimate by Irwin & Hatzidimitriou (1995) ( $28'$ ). However, the absence of plateaus in the density profiles at large galacto-centric distances and the fact that the scale-length along the semi-major axis and semi-minor axis (re-scaled to semi-major axis units using the ellipticity of the galaxy) are the same within errors, indicates that a tidal-tail is not present. More data are probably required to reach stronger conclusions in this sense.

The central surface magnitude is estimated to be  $\mu''_{V''} = 24.4 \pm 0.5$  and the core radius  $r_c = 7'5 \pm 0'3$  or  $r_c = 175 \pm 7$  kpc.

The possibility suggested by Kroupa (1997) and Kessel & Kroupa (1998) that the high velocity dispersions of dwarf spheroidal galaxies could be accounted for by adequate spatial orientations rather than being produced by large amounts of dark matter has been checked. The conclusion is that this cannot be the case for Draco. An upper limit to Draco's size along the line of sight is  $\sim 14$  kpc; less than  $1/3$  the value required by Kroupa (1997) models.

We are grateful to Dr. Kroupa, who made the results of their tridimensional models available to us and for several fruitful discussions and to Dr. Gómez-Flechoso, for several useful suggestions and discussion on the dynamical part of the paper.

This article is based on observations made with the 2.5 m Isaac Newton Telescope operated on the island of La Palma by the ING in the Spanish Observatorio del Roque de Los Muchachos of the Instituto de Astrofísica de Canarias. This research has made use of the NASA/IPAC Extragalactic Database (NED) which is operated by the Jet Propulsion Laboratory, California Institute of Technology, under contract with the National Aeronautics and Space Administration. This research has been supported by the Instituto de Astrofísica de Canarias (grant P3/94), and the General Directorates of Research of the Kingdom of Spain (grant PI97-1438-C02-01), and of the autonomous government of the Canary Islands (grant PI1999/008).

## REFERENCES

Aaronson, M., & Mould, J. 1980, *ApJ*, 240, 804

Alcaino, G., Liller, W., Alvarado, F., & Wenderoth, E. 1990, *AJ*, 99, 183

Alcaino, G., Liller, W., Alvarado, F., & Wenderoth, E. 1994, *AJ*, 107, 230

Alcaino, G., Liller, W., Alvarado, F., Mironov, A., Ipatov, A., Piskunov, A., Samus, N., & Smirnov, O. 1999, *A&AS*, 136, 461

Aparicio, A. 1998, in IAU Symp. 192, *The stellar content of the Local Group*, ed. Whitelock, & Cannon (San Francisco: ASP), 107

Aparicio, A. 2001, in *Observed HR diagrams and stellar evolution: the interplay between observational constraints and theory*, ed. J. Fernandes and T. Lejeune, ASP conference series, in press

Aparicio, A., & Gallart, C. 1995, *AJ*, 110, 2105

Aparicio, A., Gallart, C., & Bertelli, G. 1997, *AJ*, 114, 680

Azzopardi, M., Lequeux, J., & Westerlund, B. E. 1986, *A&A*, 161, 232

Baade, W. 1963, *Evolution of Stars and Galaxies*, ed. C. Payne-Gaposchkin (Cambridge: MIT Press)

Baade, W., & Swope, H. H. 1961, *AJ*, 66, 300

Behr, B. B., Djorgovski, S. G., Cohen, J. G., McCarthy, J. K., Côté, P., Piotto, G., & Zoccali, M. 2000, *ApJ*, 528, 849

Bertelli, G., Bressan, A., Chiosi, C., Fagotto, F., & Nasi, E. 1994, *A&AS*, 106, 275

Carney, B. W., & Seitzer, P. 1986, *AJ*, 92, 23

Carretta, E., & Gratton, R. 1997, *A&AS*, 121, 95 (CG)

Davidge, T. J. 1994, *AJ*, 108, 2123

Demarque, P., & Hirshfeld, A. W. 1975, *ApJ*, 202, 346

Elston, D., & Silva, D. R. 1992, *AJ*, 104, 1360

Freedman, W. L. 1992, *AJ*, 104, 1349

Frogel, J. A., Blanco, V. M., Cohen, J. G., & McCarthy, M. F. 1982, *ApJ*, 252, 133

Gallagher, J. S., Wyse, R. F. G. 1994, *PASP*, 106, 1225

Gallart, C. 2001, in *Observed HR diagrams and stellar evolution: the interplay between observational constraints and theory*, ed. J. Fernandes and T. Lejeune, ASP conference series, in press

Gallart, C., Aparicio, A., Vílchez, J. M., 1996, *AJ*, 112, 1928

Gallart, C., *et al.* 1999a, *ApJ*, 514, 665

Gallart, C., Freedman, W. L., Aparicio, A., Bertelli, G., & Chiosi, C. 1999b, AJ, 118, 2245  
Grillmair, C. J., *et al.* 1998, AJ, 115, 144  
Hernández, X., Gilmore, G., & Valls-Gabaud, D. 2000, MNRAS, 317, 831  
Hodge, P. W. 1964, AJ, 69, 853  
Hurley-Keller, D., Mateo, M., & Nemec, J. 1998, AJ, 115, 1840  
Irwin, M. & Hatzidimitriou, D. 1995, MNRAS, 277, 1354  
Johnston, K. V., Sigurdsson, S., & Hernquist, L. 1999, MNRAS, 302, 771  
Klessen, R. S., & Kroupa, P. 1998, ApJ, 498, 143  
Kroupa, P. 1997, New Astronomy, 2, 139  
Kroupa, P. Tout, C. A., & Gilmore, G. 1993, MNRAS, 262, 545  
Lake, G. 1990, MNRAS, 244, 701  
Lee, M. G., Freedman, W. L., & Madore, B. F. 1993, AJ, 106, 964  
Lee, Y.-W., Yoon, S.-K., Lee, H.-C., & Woo, J.-H. 1999, in ASP Conf. Proc., Vol. 192, *Spectrophotometric Dating of Stars and Galaxies*, Edited by I. Hubeny, S. Heap, & R. Cornett (San Francisco: ASP), 185  
Martínez-Delgado, D., Alonso-Graciá, J., Aparicio, A., & Gómez-Flechoso, M. A. 2001b, ApJ, 549, L63  
Martínez-Delgado, D., & Aparicio, A. 1997, ApJ, 480, L107  
Martínez-Delgado, Aparicio, A., Gómez-Flechoso, M. A., & Carrera, R. 2001a, ApJ, 549, L199  
Martínez-Delgado, D., Gallart, C., & Aparicio, A. 1999, AJ, 118, 862  
Mateo, M. 1998, ARA&A, 36, 455  
Mateo, M., Olszewski, E. W., & Morrison, H. L. 1998, ApJ, 508, L55  
Mighell, K. J., & Rich, R. M. 1996, AJ, 111, 777  
Mighell, K. J. 1997, AJ, 114, 1458  
Mould, J., & Aaronson, M. 1983, ApJ, 273, 530  
Mould, J. R., Cannon, R. D., Frogel, J. A., & Aaronson, M. 1982, ApJ, 254, 500  
Nemec, J. M. 1984, in IAU Symp. 105, *Observational Tests of the Stellar Evolution Theory*, ed. A. Maeder & A. Renzini (Dordrecht: Reidel), 465  
Norris, J., & Zinn, R. 1975, ApJ, 202, 335  
Piatek, S., Pryor, C., Armandroff, T. E., & Olszewski, E. W. 2001, AJ, 121, 841  
Pryor, C. & Kormendi, J. 1990, AJ, 100, 127  
Rosenberg, A., Saviane, I., Piotto, G., & Aparicio, A. 1999, AJ, 118, 2306

Saviane, I., Rosenberg, A., Piotto, G., Aparicio, A. 2000, A&A, 355, 966  
Schlegel, D. J., Finkbeiner, D. P., & Davis, M. 1998, ApJ, 500, 525  
Shetrone, M. D., Bolte, M., & Stetson, P. B. 1998, AJ, 115, 1888  
Stetson, P. B. 1979a, AJ, 84, 1149  
Stetson, P. B. 1979b, AJ, 84, 1167  
Stetson, P. B. 1984, PASP, 96, 128  
Stetson, P. B. 1994, PASP, 106, 250  
Stetson, P. B. & Harris, W. E. 1988, AJ, 96, 909  
Stetson, P. B., Hesser, J.E. & Smecker-Hane, T.A. 1998, PASP, 110, 533  
Stetson, P. B., VandenBergh, D. A., & McClure, R. 1985, PASP, 97, 908  
White, S. D. M., & Rees, M. J. 1978, MNRAS, 183, 341  
Wilson, A. G. 1955, PASP, 67, 27  
Yi, S., Demarque, O., & Oemler, A. 1997, ApJ, 486, 201  
Zinn, R., & Searle, L. 1976, ApJ, 209, 734  
Zinn, R., & West, M. J. 1984, ApJS, 55, 45 (ZW)

Table 1. Journal of observations

Date	Draco Field	Time (UT)	Filter	Exp. time (s)
98.05.29	A	00:01	<i>B</i>	900
98.05.29	A	00:19	<i>B</i>	900
98.05.29	A	00:37	<i>R</i>	550
98.08.20	A	21:38	<i>R</i>	30
98.08.20	A	21:42	<i>R</i>	900
99.06.16	A	02:05	<i>B</i>	120
99.06.16	A	02:12	<i>R</i>	120
00.06.09	B	02:29	<i>B</i>	900
00.06.09	B	02:45	<i>B</i>	900
00.06.09	B	03:01	<i>B</i>	900
00.06.09	B	03:16	<i>B</i>	900
00.06.09	B	03:33	<i>R</i>	600
00.06.09	B	03:33	<i>R</i>	600
00.06.09	B	03:43	<i>R</i>	600
00.06.09	B	03:54	<i>R</i>	600
00.06.09	B	04:05	<i>R</i>	600
00.06.09	B	04:16	<i>R</i>	600
00.06.09	B	04:27	<i>R</i>	600
00.09.23	C	20:24	<i>R</i>	120
00.09.23	C	20:28	<i>R</i>	900
00.09.23	C	20:44	<i>R</i>	900
00.09.23	C	21:00	<i>R</i>	900
00.09.23	C	21:17	<i>B</i>	120
00.09.23	C	21:20	<i>B</i>	900
00.09.23	C	21:36	<i>B</i>	900
00.09.23	C	21:52	<i>B</i>	900

Table 2. Globular clusters used for the metallicity calibration in the  $[M_R, (B - R)]$  plane

Cluster	Metallicity		Distance	$E(B - V)$
	ZW	CG		
NGC 1904	−1.7	−1.4	15.59	0.01
NGC 4590	−2.1	−2.0	15.19	0.05
NGC 6723	−1.1	−1.0	14.85	0.05

Table 3. Coefficients of the metallicity scales calibration

Metallicity scale	a	b	c
ZW	1.924	−5.199	...
CG	−3.013	13.192	−15.429

Table 4. Density profile scales

Stellar population	$\alpha(')$
All stars, full annuli	$4.7 \pm 0.3$
All stars, semi-major axis	$5.3 \pm 0.5$
All stars, semi-minor axis <sup>(1)</sup>	$5.2 \pm 0.4$
MS, full annuli	$5.0 \pm 0.1$
MS, semi-major axis	$4.8 \pm 0.3$
MS, semi-minor axis <sup>(1)</sup>	$5.2 \pm 0.4$
RGB, full annuli	$5.9 \pm 0.4$
RGB, semi-major axis	$5.1 \pm 0.6$
RGB, semi-minor axis <sup>(1)</sup>	$5.9 \pm 0.5$

Note. — <sup>(1)</sup> Parameters given for semi-minor axis have been scaled onto semi-major axis units; i.e., they have been divided by  $b/a$ .

Table 5. Morphological and integrated parameters of Draco

Parameter	Value
$\alpha_{00}$	17 <sup>h</sup> 20 <sup>m</sup> .3
$\delta_{00}$	57°55'
$\mu''V'',0$	$24.4 \pm 0.5$
$\mu_{B,0}$	$25.0 \pm 0.5$
$\mu_{R,0}$	$23.9 \pm 0.5$
$\alpha$	$5'.0 \pm 0'.1$
$r_c$	$7'.5 \pm 0'.3$
	( $175 \pm 7$ kpc)
$d$	$80 \pm 7$ kpc
[Fe/H]	$-1.8 \pm 0.2$
$''V''_T$	$10.1 \pm 0.5$
$B_T$	$10.6 \pm 0.5$
$R_T$	$9.6 \pm 0.5$
$M''V''$	$-9.4 \pm 0.5$
$M_B$	$-8.9 \pm 0.5$
$M_R$	$-9.9 \pm 0.5$
$L''V'' (L_\odot)$	$4.7 \times 10^5$
$M_{VT} (M_\odot)$	$22 \times 10^6$
$M_{VT}/L''V'' (M_\odot/L_\odot)$	47
$M_\star(a < 7'.5) (M_\odot)$	$2.1 \times 10^5$
$M_\star(a < 30') (M_\odot)$	$4.3 \times 10^5$
$M_\star(a < 42') (M_\odot)$	$5.3 \times 10^5$
$\kappa = 1 - (M_\star(a < 42')/M_{VT})$	0.98

Table 6. Comparison of morphological parameters

Reference	$r_c$ (')	$r_t$ (')
Hodge (1964)	6.5	$26 \pm 2$
Irwin & Hatzidimitriou (1990)	$9.0 \pm 0.7$	$28.3 \pm 2.4$
Lake (1990)	$7.0 \pm 2.5$	55
Pryor & Kormendy (1990)	7.1	36
This work	$7.5 \pm 0.3$	42

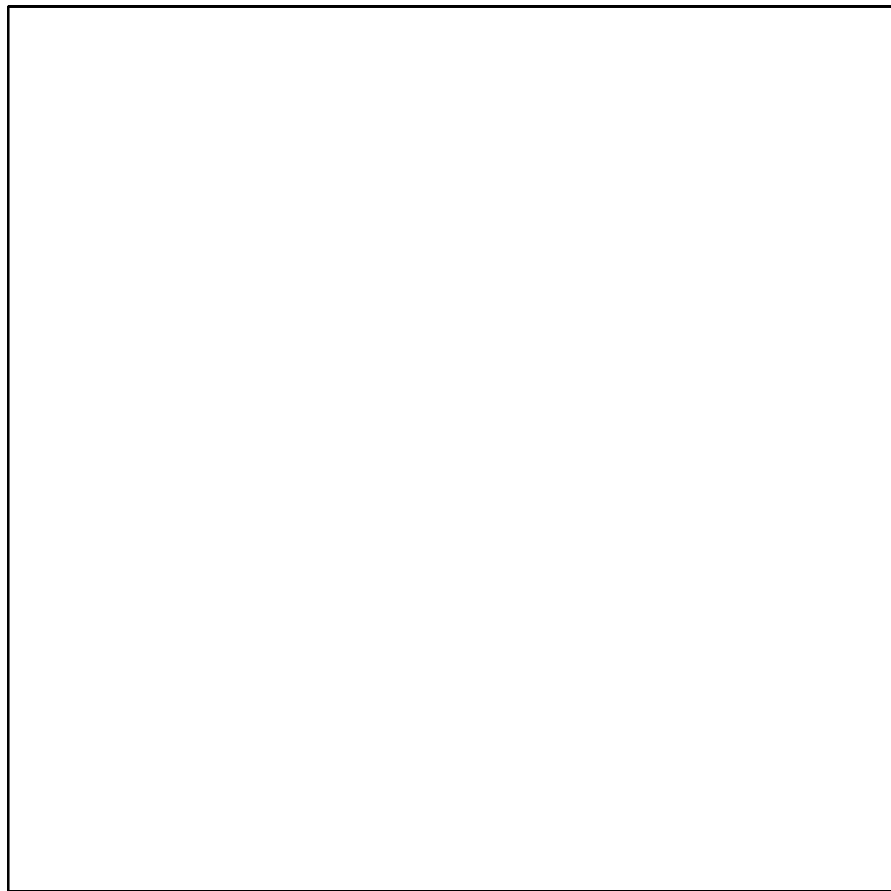


Fig. 1.— Digitized Sky Survey image of Draco. The observed fields are shown. North is up, East is left.

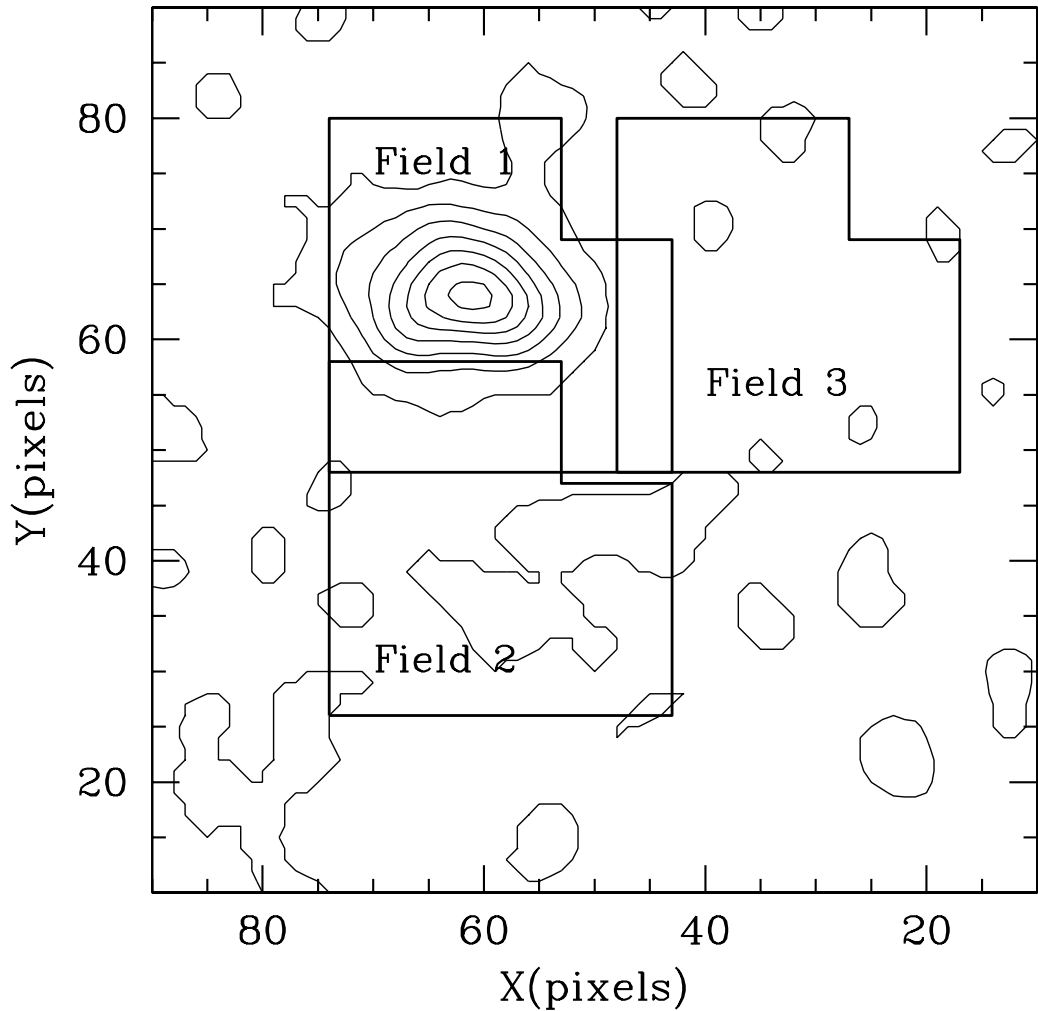


Fig. 2.— Isopleth map of Draco taken from Irwin & Hatzidimitriou (1995). Coordinates refer to the scales given by these authors. The observed fields are shown. North is up, East is left.

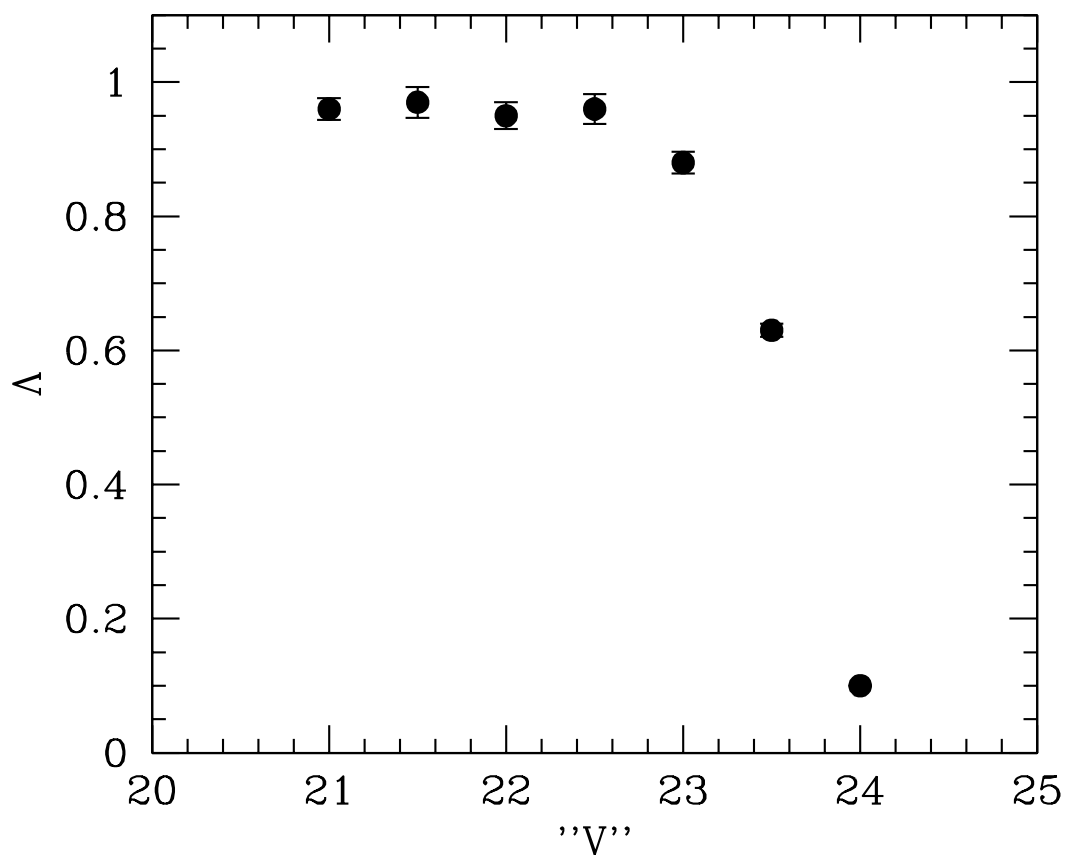


Fig. 3.— The completeness factor as a function of "V" for field 1.

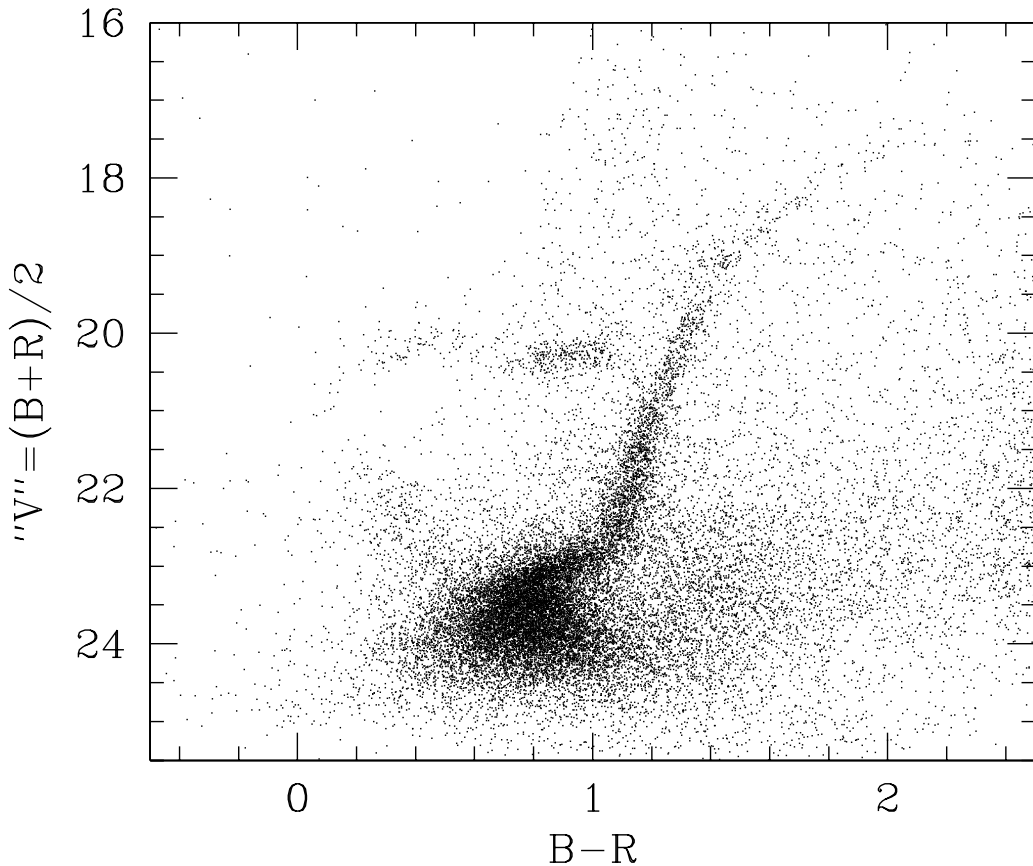


Fig. 4.— The CMD of Draco. Stars within the inner  $30'$  (semi-major axis) are plotted. Beside a well populated MS and a steep RGB, indicative of relatively low metallicity, the most significant features are the extended blue plume and the mainly red HB. Some blue HB stars and an AGB sequence are also visible.

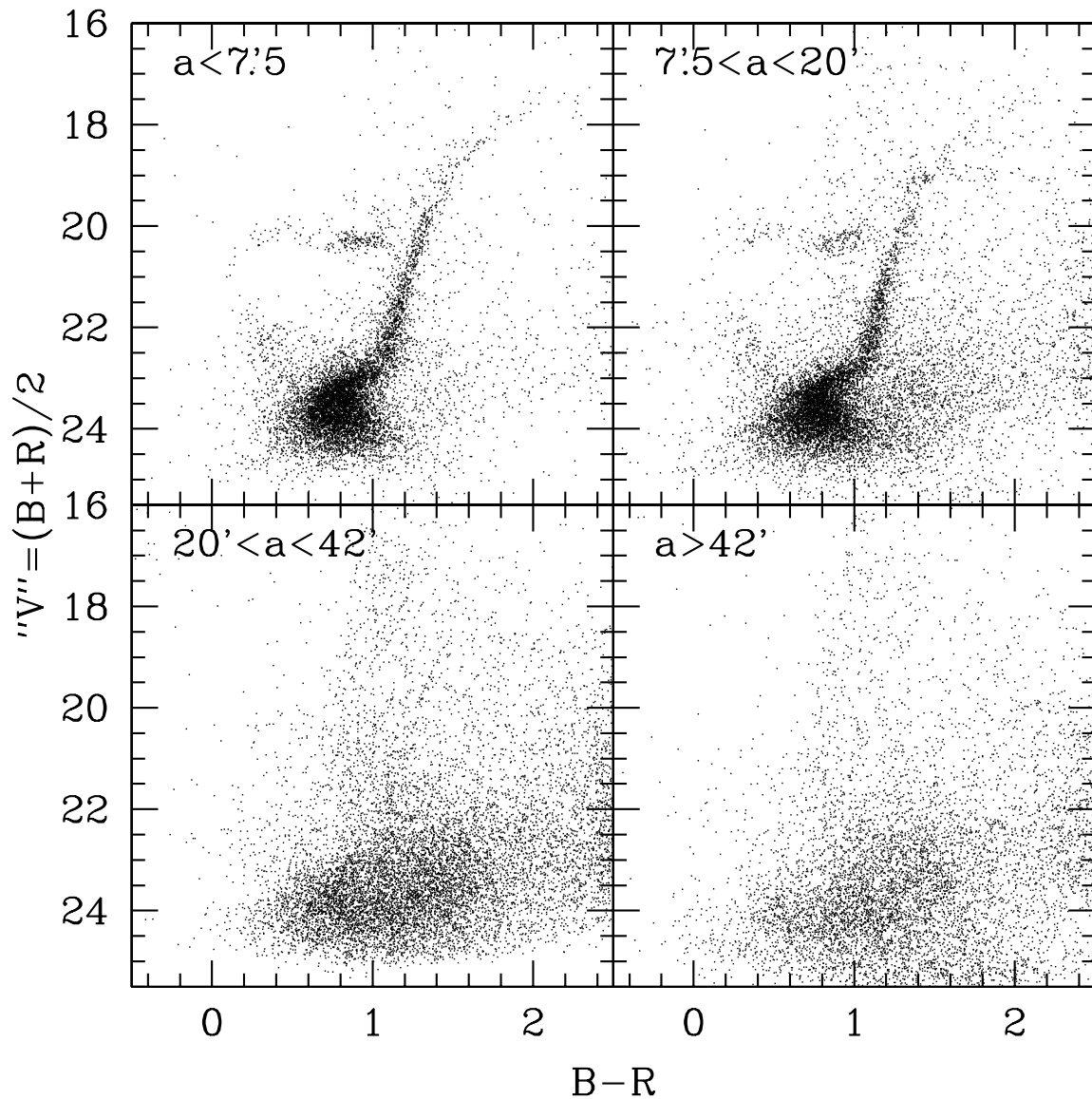


Fig. 5.— CMDs of four elliptical annuli centered on the center of Draco and of semi-major axis as indicated.

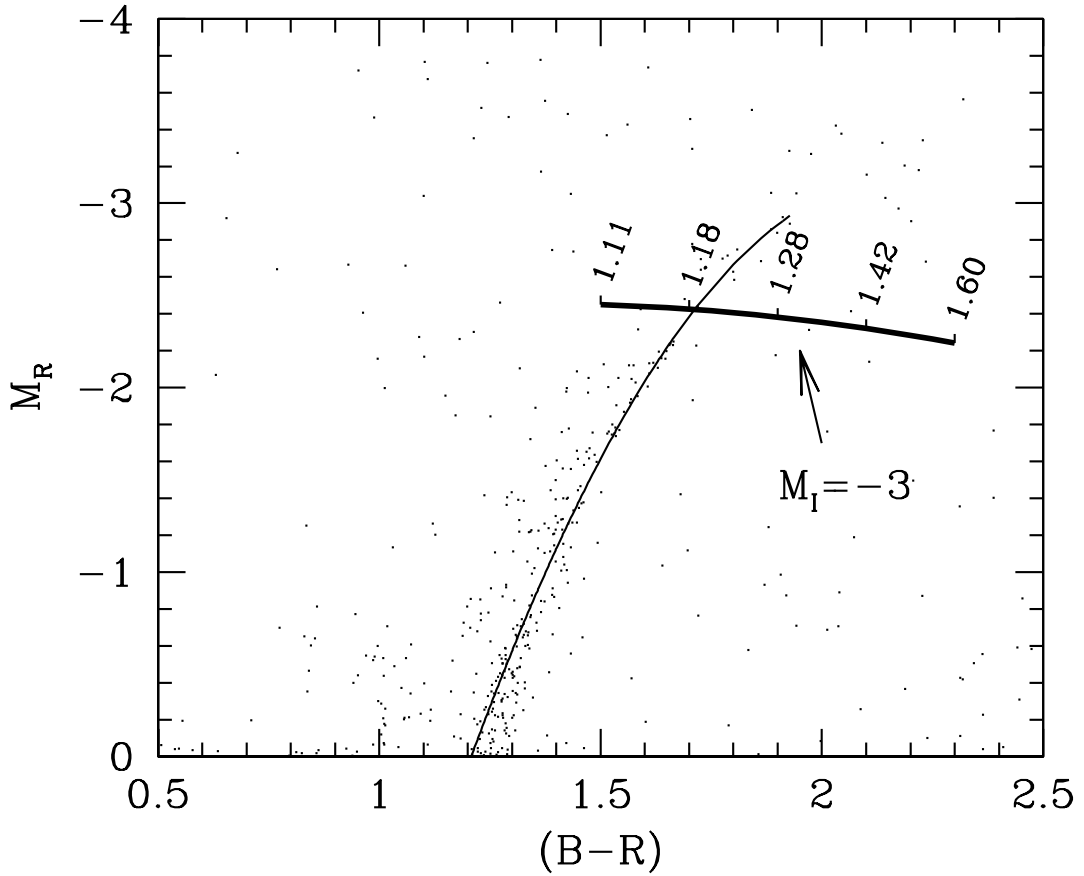


Fig. 6.— The upper part of the Draco RGB. Only stars in the inner  $10'$  have been plotted. The thick track shows the line of constant absolute  $I$  magnitude for  $M_I = -3$ . The curve has been calculated using a synthetic CMD. The scale plotted on the line shows the values of  $(V - I)_{I=-3}$  along it. The fiducial RGB of Draco is shown by the thin line. The point where this line crosses the curve provides  $(V - I)_{I=-3}$  for Draco, from which the metallicity can be estimated.

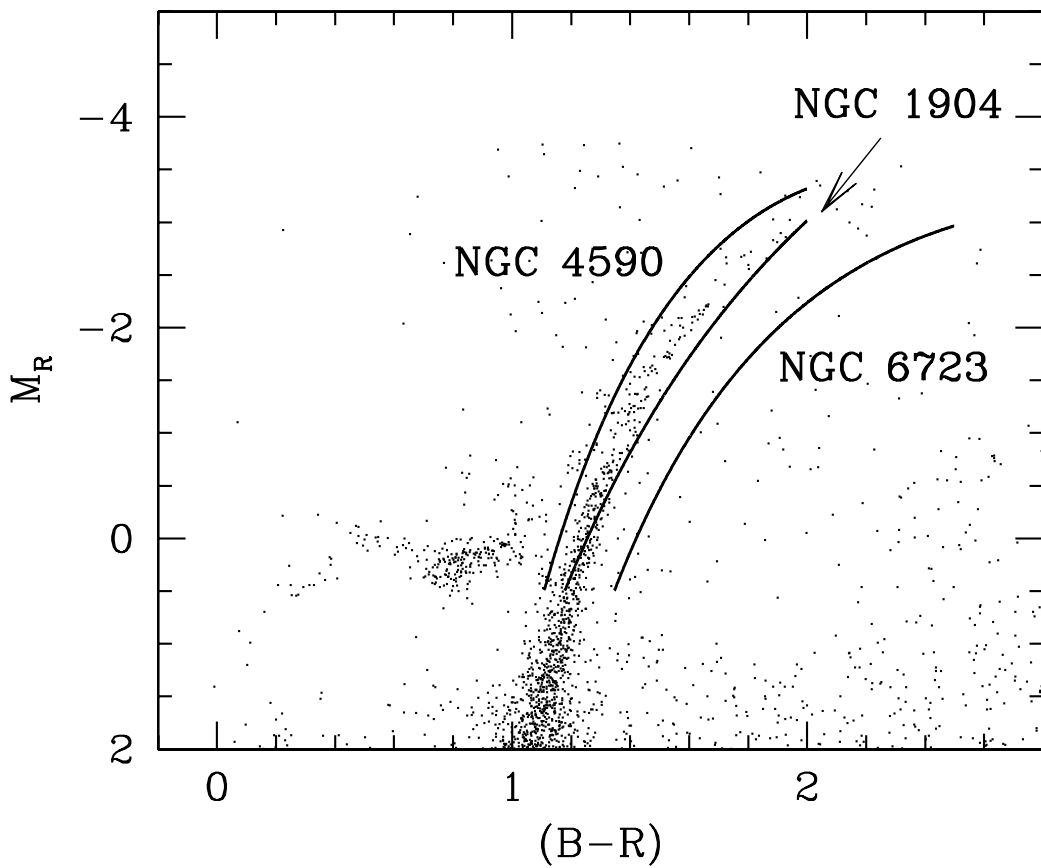


Fig. 7.— The fiducial RGBs of the three globular clusters used to set the metallicity calibration in the  $[M_R, (B - R)]$  plane discussed in the text are shown superimposed on the CMD of Draco (inner  $10'$ ). This shows that the metallicity of Draco is probably between those of NGC 4590 and NGC 1904.

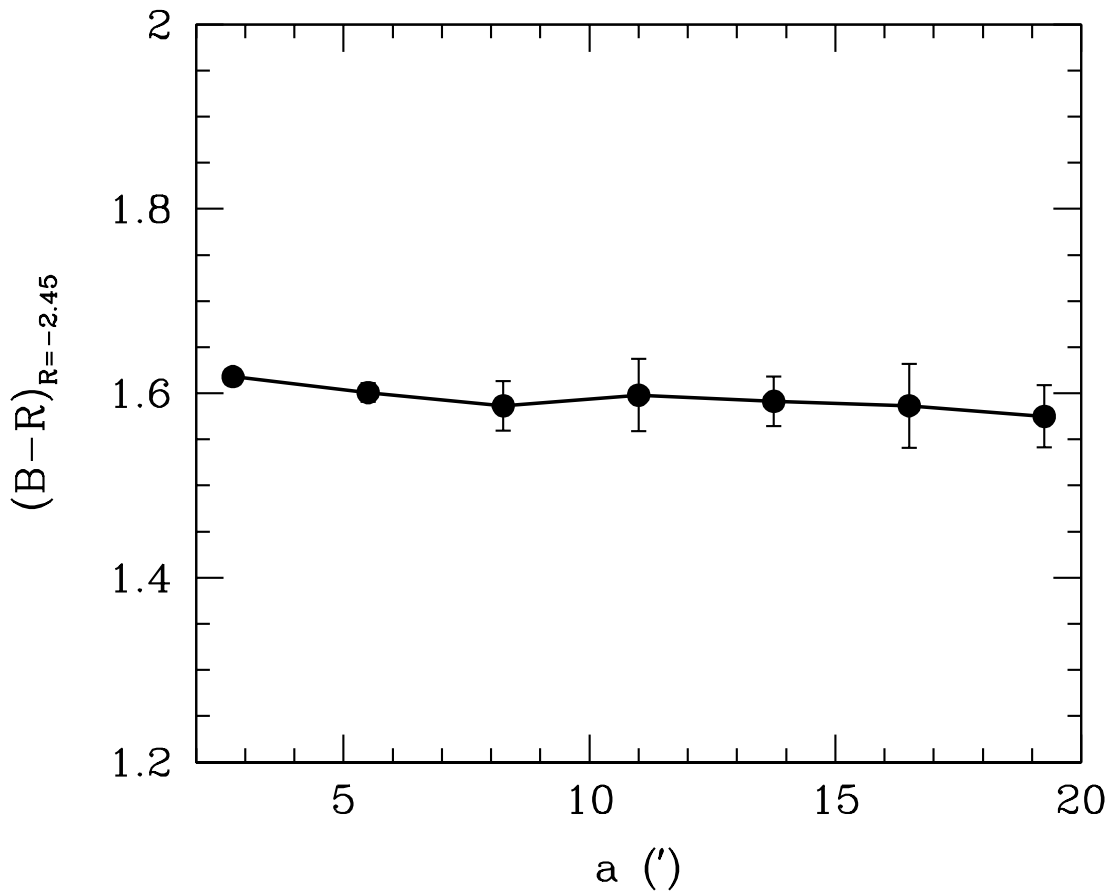


Fig. 8.—  $(B - R)_{R=-2.45}$  (the color of the RGB measured at  $M_R = -2.45$ ) of Draco stars for elliptical annuli of increasing size. If a metallicity gradient should exist in Draco it would be put into evidence by a gradient of  $(B - R)_{R=-2.45}$ .

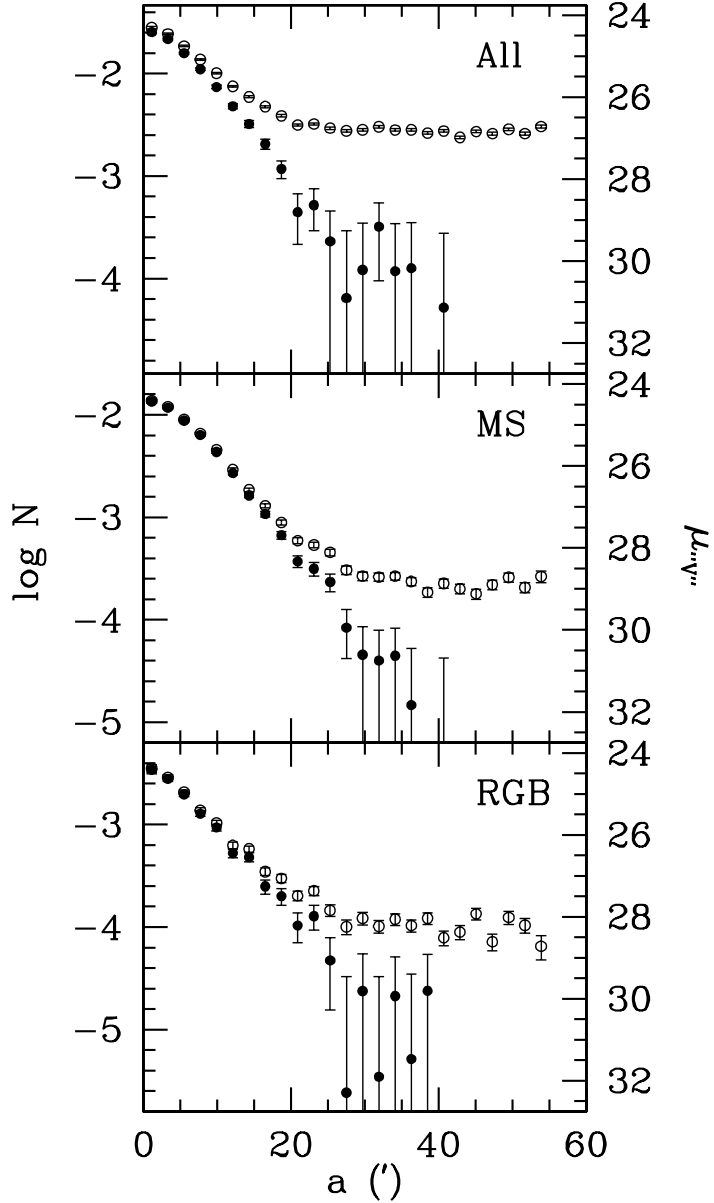


Fig. 9.— Surface star density and surface magnitude distributions in Draco. All the resolved stars have been considered to plot the upper panel figure, while only MS and RGB stars have been respectively used for the medium and lower panel figures. Stars have been counted in elliptical annuli of eccentricity  $1 - a/b = 0.29$ , position angle  $82^\circ$  and increasing semi-major axis. Horizontal axis gives the semimajor-axis in arcmin. Left-hand vertical axis gives the logarithm of the star density per  $\text{arcsec}^2$ . The right-hand vertical axis gives an estimate of the surface magnitude, calibrated as described in text. Open circles represent the raw density distribution. Filled circles show the density distribution after subtraction of the sky foreground contamination, estimated as described in text.

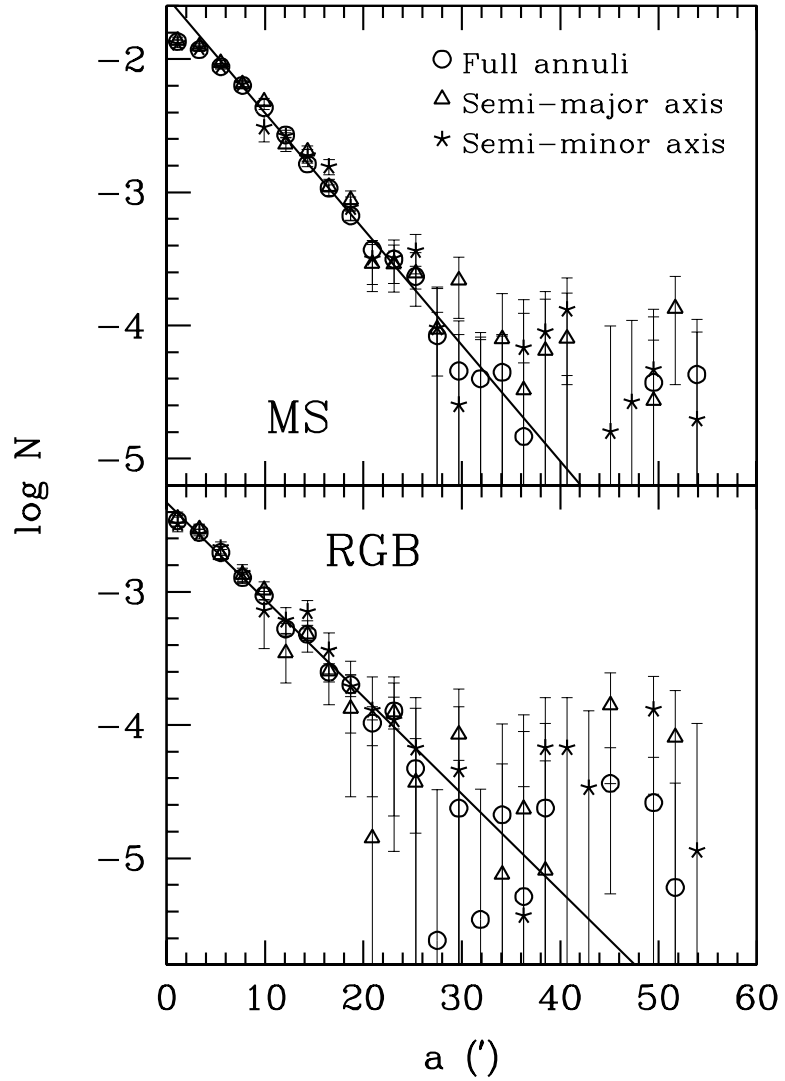


Fig. 10.— Surface star density of stars along the semi-major and semi-minor axis of Draco, after correction of foreground contamination. MS (upper panel) and RGB (lower panel) stars have been considered. The density distribution obtained for star counts in the full elliptical annuli are also plotted for comparison. Straight lines show the fits done using full elliptical annuli distributions.

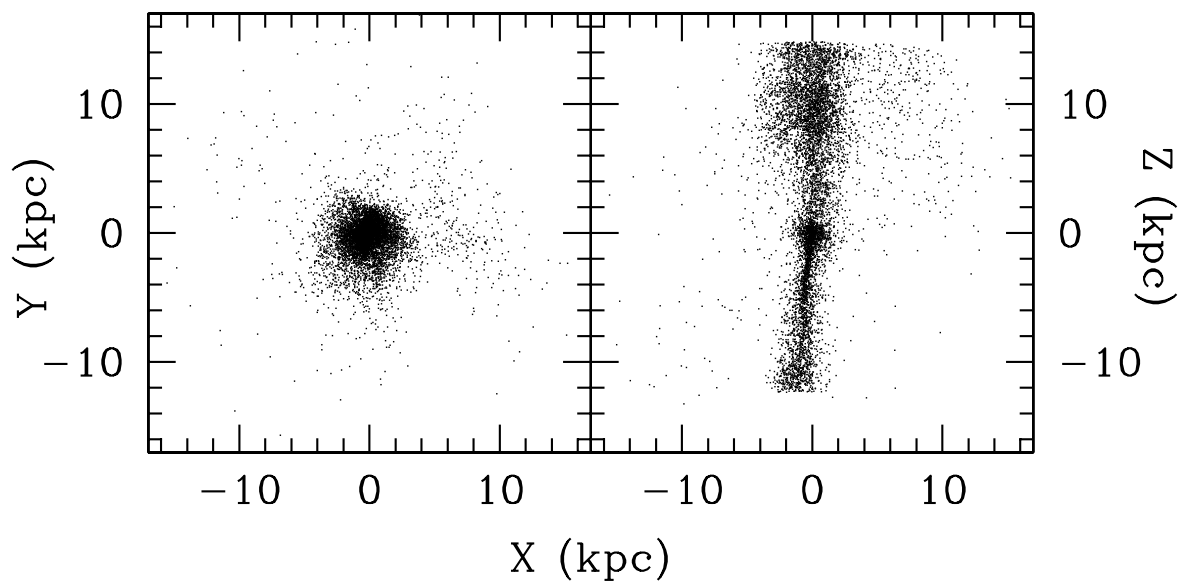


Fig. 11.— The spatial distribution of stars according to RS1-4 model of Kroupa (1997), which reproduces the velocity dispersion of Draco. The  $Z$  axis corresponds to the line of sight. Coordinates are given in kpc and are centered on the center of Draco.

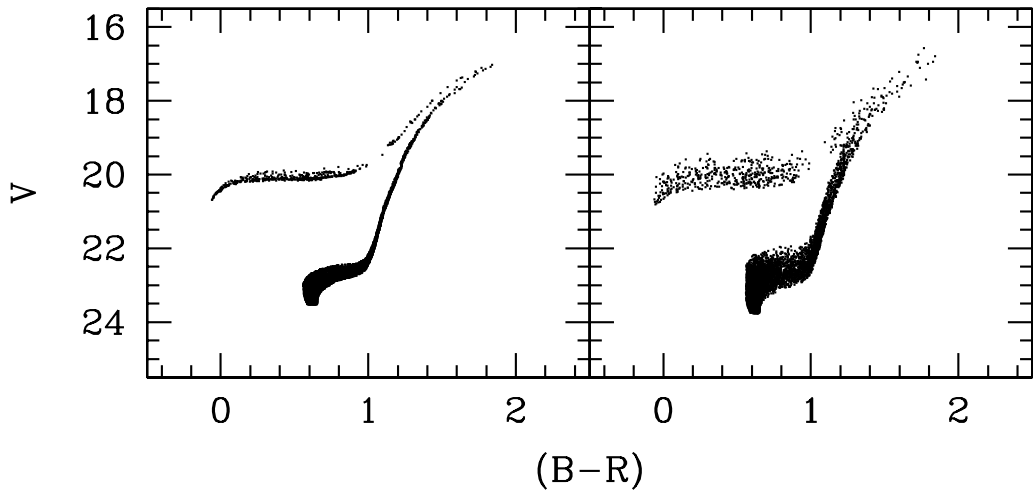


Fig. 12.— The left-hand panel shows a synthetic CMD for an old stellar population, similar to the main population found in Draco (see §4). The right-hand panel shows the same population including the simulation of the distance dispersion corresponding the RS1-4 model of Kroupa (1997), as shown in Figure 11.

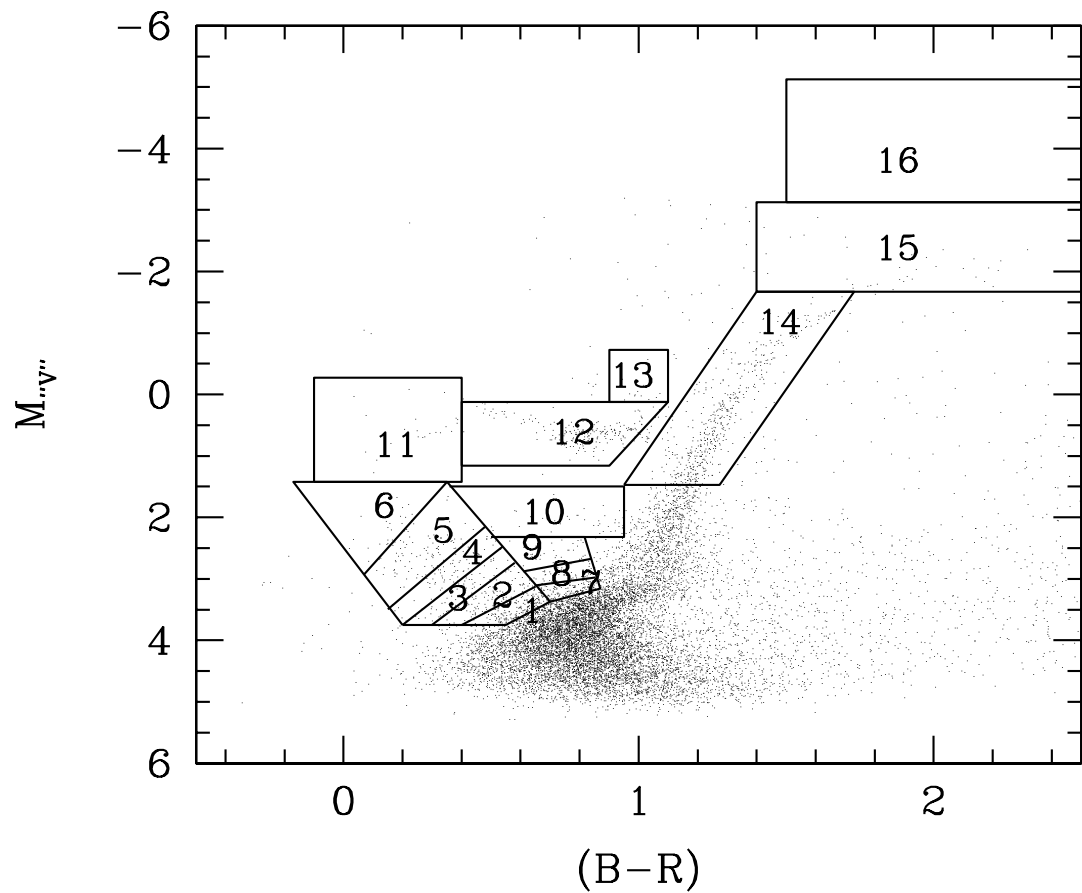


Fig. 13.— The boxes defined to sample the stellar population of Draco, overplotted on the CMD. These boxes are used to derive Draco’s SFR with the *partial model* method (see text).

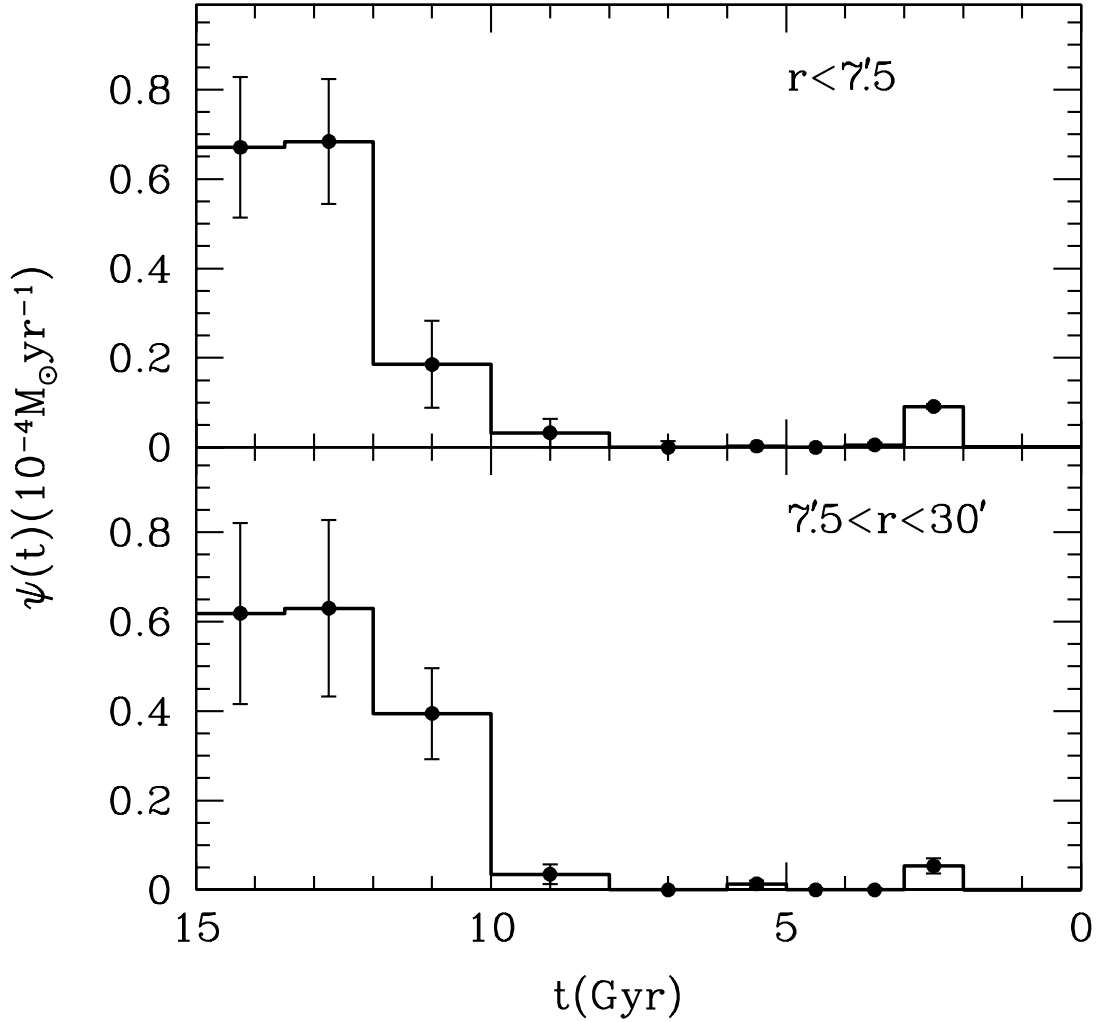


Fig. 14.— The solution for the SFR of Draco using the *partial model* method. Two solutions are given. The first for the inner  $7.5'$  and the second for the region between  $7.5'$  and  $30'$ . Error bars account for the dispersion of possible solutions for each age range.

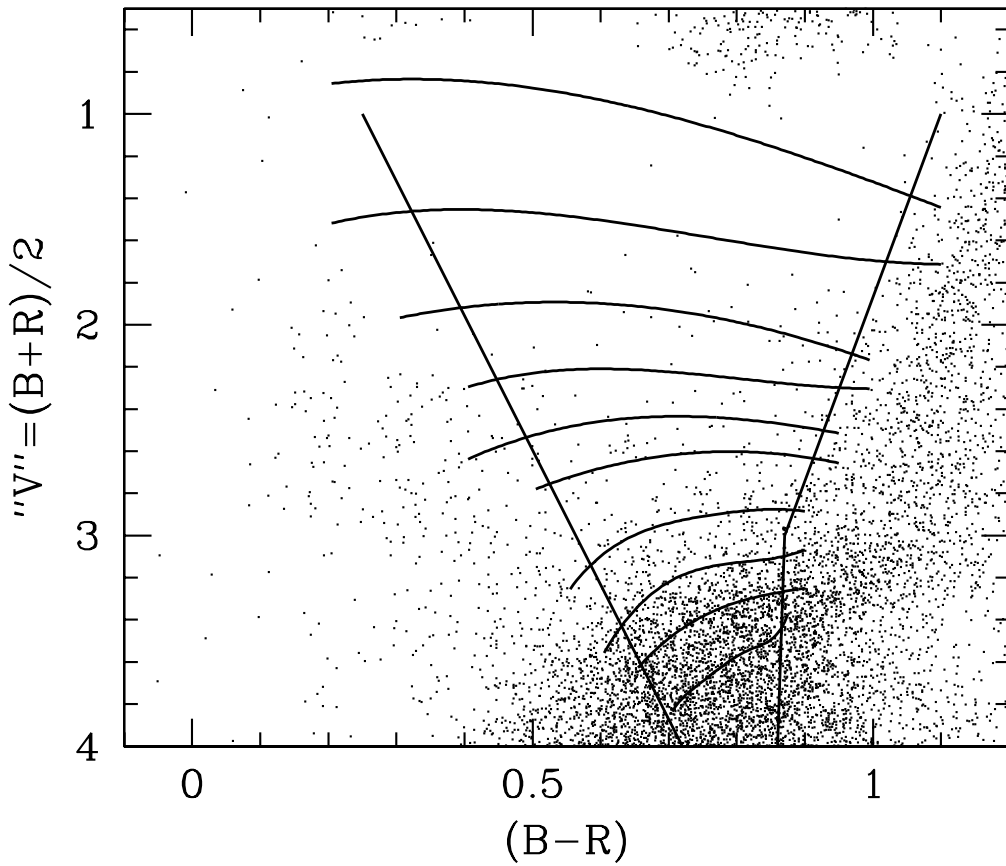


Fig. 15.— Subgiant region of Draco's CMD. Isochrones of several ages are overplotted, corresponding to the ages used to derive the SFR with the *subgiant* method (see text). From up to down, ages are 1.25, 2, 3, 4, 5, 6, 8, 10, 12 and 15 Gyr. Diagonal straight lines show the color interval used to limit the SG region.

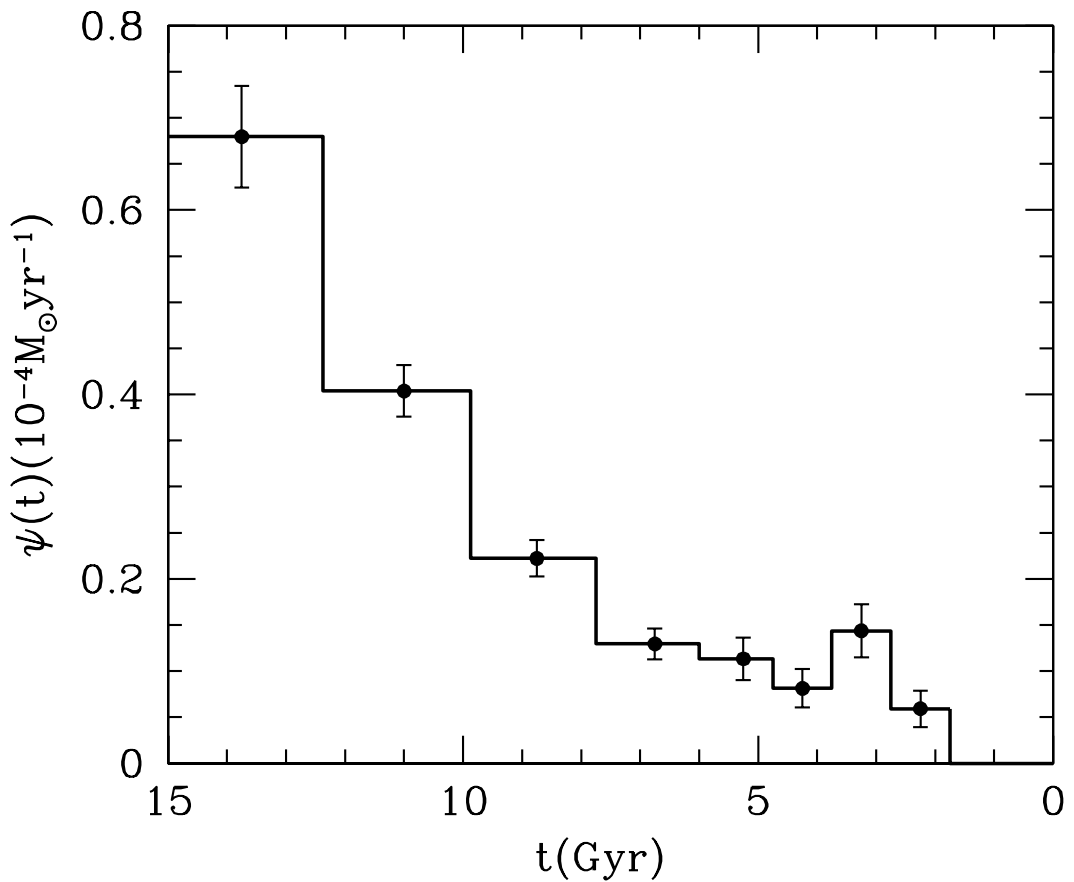


Fig. 16.— The solution for Draco's SFR using the *subgiant* method. The inner 10' (semi-major axis) have been considered.